Romarchite and Other Corrosion Phases on Metal Artifacts from the *Queen Anne's Revenge* (1718)

Stacie E. Dunkle

Thesis submitted to the Faculty of the Virginia Polytechnic Institute and State University in partial fulfillment of the requirements for the degree of

Master of Science

in

Geological Sciences

James R. Craig, Chair
J. Donald Rimstidt
Wayne R. Lusardi

April 19, 2002
Blacksburg, Virginia

Keywords: Romarchite, *Queen Anne's Revenge*, Tin, Metal Artifacts, Pewter, Abhurite, Corrosion

Romarchite and Other Corrosion Phases on Metal Artifacts from the *Queen Anne's Revenge* (1718)

Stacie E. Dunkle

(abstract)

Metal artifacts from the pirate Blackbeard's flagship, *Queen Anne's Revenge* (1718), were studied and a preliminary assessment of the corrosion products that have formed on them is presented. Artifacts made of iron, lead, tin, copper, mercury, gold, and silver were recovered from the site with only those made of precious metals displaying no corrosion products. Detailed analysis was conducted of the surfaces of pewter artifacts, made from a tin-rich alloy, revealing corrosion products composed of romarchite (SnO), hydroromarchite ($5SnO{\cdot}2H_2O$), and abhurite ($Sn_3O(OH)_2Cl_2$). For comparison, corroded pewter artifacts originating from five other archaeological sites submerged in seawater, dating to between ~1550 and 1733, were analyzed. All of these samples also exhibit abhurite, romarchite, and hydroromarchite, however, some of the artifacts also display cassiterite (SnO_2). Textural analysis indicates that abhurite is the first alteration product to arise, followed by romarchite and hydroromarchite and, in some cases, ending with the formation of cassiterite. The absence of cassiterite on many samples demonstrates that, while appearing to be stable under the conditions that were present, the phase has not yet had time to form. Because of the very limited stability field for romarchite, its presence on these artifacts seems to be the result of a kinetic effect, while its universal appearance suggests that it is a required step in the oxidation of pure tin to the final most stable phase of cassiterite. Knowledge of the stability of pewter corrosion products and their effectiveness as agents of passivation can provide insight into the processes of tin corrosion.

ACKNOWLEDGEMENTS

I would like to thank the Underwater Archaeology Branch of the North Carolina Department of Cultural Resources for providing samples from the *Queen Anne's Revenge* and for encouraging detailed analysis and comparison with other samples. Thank you also for providing the majority of the artifact images presented in this thesis. I would also like to thank Dr. Donny Hamilton for donating samples from Port Royal, Jamaica, Robert Benson for *La Capitana* (1715) samples and David Moore for *Henrietta Marie* (1701) and St Johns Bahamas (~1550) samples. For *San Jose* (1733) samples, I would like to thank both the Division of Historical Resources of the Florida Department of State as well as Joe Kimbell. In addition, I would like to thank Dr. Robert Tracy and Dr. Gretchen Benedix, for training and maintenance of the SEM and electron microprobe, and Dr. Ross Angel, for training and assistance with x-ray diffraction. Thanks to the Horton Foundation for providing financial support for travel beneficial to this research.

In addition, I would like to acknowledge my committee members Dr. J. Donald Rimstidt, for assistance with thermodynamic calculations, and Wayne Lusardi, for assistance with anything archaeological. Dr. James R. Craig deserves a huge amount of thanks for his creativity in advising me through a successful masters thesis based on the geochemistry of human interaction with the natural environment and the mystique of Blackbeard the pirate. Although time has passed quickly, it is difficult to believe that my first visit to Blacksburg was only two years ago. Thanks for giving me the opportunity to live and study here.

I would also like to thank all of my family and friends who have made it through this experience with me! I could not have done this without you. We've had great fun and I know I have made lifelong friends during my time in Blacksburg. My biggest thanks of all goes to Rob, Kiwi and Captain for making me smile every day.

TABLE OF CONTENTS

ABSTRACT……. ii
ACKNOWLEDGEMENTS…… iii
LIST OF FIGURES……vi
LIST OF TABLES……... viii
INTRODUCTION……... 1

CHAPTER I: THE CORROSION MINERALOGY OF METAL ARTIFACTS FROM THE *QUEEN ANNE'S REVENGE* (1718)

ABSTRACT……...2
INTRODUCTION…… 2
IRON……..3
LEAD……4
TIN……5
COPPER…… 7
MERCURY……8
GOLD AND SILVER……... 9
SUMMARY……...11

CHAPTER II: ROMARCHITE AND ASSOCIATED PHASES FORMED DURING THE CORROSION OF PEWTER ARTIFACTS FROM THE *QUEEN ANNE'S REVENGE* (1718)

ABSTRACT……...12
INTRODUCTION…… 12
SCOPE OF STUDY……...14
SAMPLE ANALYSIS……...15
RESULTS……... 15
DISCUSSION…… 19
CONCLUSION……..21

CHAPTER III: ROMARCHITE AND ASSOCIATED PHASES AS COMMON CORROSION PRODUCTS ON PEWTER ARTIFACTS

ABSTRACT……...23
INTRODUCTION…… 23
SCOPE OF STUDY……...26
SAMPLE ANALYSIS……...26
RESULTS
Pewter from the *Queen Anne's Revenge* (1718)…… 27
Pewter from the St. Johns Bahamas site (~1550)…….. 29
Pewter from *La Capitana* (1715)……...31
Pewter from the *San José* (1733)……...34
Pewter from Port Royal, Jamaica (1692)……...…….... 35

Pewter from the *Henrietta Marie* (1701)……...35
DISCUSSION……38
CONCLUSION……. 41

REFERENCES…….43
APPENDIX A: Microprobe Data of Pewter Artifacts and Corrosion Products ……45
VITA……..56

LIST OF FIGURES

CHAPTER I: THE CORROSION MINERALOGY OF METAL ARTIFACTS FROM THE *QUEEN ANNE'S REVENGE* (1718)

Figure 1.1: Iron nails……..3
Figure 1.2: Polished cross section of an iron nail…… 3
Figure 1.3: Iron disulfide precipitated on the outside surface of quartz sand grains. 4
Figure 1.4: Lead shot of various sizes……... 4
Figure 1.5: Polished cross section of a lead shot concretion… 5
Figure 1.6: The recovery of a pewter charger by Wayne Lusardi……. 6
Figure 1.7: Corrosion phases on a polished cross section of a pewter artifact…….. 6
Figure 1.8: Universal staff mount made of brass……... 7
Figure 1.9: Crystals of copper oxide……..7
Figure 1.10: Brass straight pins…… 8
Figure 1.11: Surface of a brass pin showing copper and zinc oxides…… 8
Figure 1.12: Contents from within the pewter syringe…….. 9
Figure 1.13: Gold grains…… 9
Figure 1.14: Polished cross section of gold placer grains……..10
Figure 1.15: Gypsum from within the pewter syringe……... 11

CHAPTER II: ROMARCHITE AND ASSOCIATED PHASES FORMED DURING THE CORROSION OF PEWTER ARTIFACTS FROM THE *QUEEN ANNE'S REVENGE* (1718)

Figure 2.1: Map showing modern location of the *Queen Anne's Revenge.*…… 13
Figure 2.2: Pewter artifacts recovered from the *Queen Anne's Revenge*…….. 14
Figure 2.3: Backscattered electron image of a polished surface of pewter……... 16
Figure 2.4: Needles of romarchite (SnO)…….. 16
Figure 2.5: Corrosion phases on polished cross sections of pewter artifacts…….18
Figure 2.6: Tin sulfide mineral on contents from within the pewter syringe…… 19
Figure 2.7: The Sn-O-H_2O system…….20
Figure 2.8: Distribution of hydrolysis products in a solution saturated with $SnO_{(s)}$..21
Figure 2.9: Expanded view of $Sn(OH)_2^o$ field from Figure 2.7.…… 22

CHAPTER III: ROMARCHITE AND ASSOCIATED PHASES AS COMMON CORROSION PRODUCTS ON PEWTER ARTIFACTS

Figure 3.1: Images of pewter artifacts……... 24
Figure 3.2: Map showing locations and dates of archaeological sites……...25
Figure 3.3: Texture of a pewter artifact from the *Queen Anne's Revenge* (1718)….27
Figure 3.4: Polished cross section of a pewter artifact from the *Queen Anne's Revenge* (1718)…….. 28
Figure 3.5: SEM photograph of romarchite precipitating on quartz sand grains…...28

Figure 3.6: Polished cross section of a pewter artifact from the St. Johns Bahamas wreck (~1550)……31
Figure 3.7: Polished cross section of a pewter artifact from *La Capitana* (1715)….33
Figure 3.8: Polished cross section of a pewter artifact from the *San José* (1733)….33
Figure 3.9: Polished cross section of a pewter artifact from Port Royal, Jamaica (1692)……35
Figure 3.10: Polished cross section of a pewter artifact from the *Henrietta Marie* (1701)……38
Figure 3.11: The Sn-O-H_2O system……...39
Figure 3.12: Distribution of hydrolysis products in solution saturated with SnO(s).40
Figure 3.13: Expanded view of $Sn(OH)_2^o$ field……41

LIST OF TABLES

CHAPTER I: THE CORROSION MINERALOGY OF METAL ARTIFACTS FROM THE *QUEEN ANNE'S REVENGE* (1718)

Table 1.1: Summary of the metal artifacts and corrosion products found at the wreck site of the *Queen Anne's Revenge*(1718)…… 10

CHAPTER II: ROMARCHITE AND ASSOCIATED PHASES FORMED DURING THE CORROSION OF PEWTER ARTIFACTS FROM THE *QUEEN ANNE'S REVENGE* (1718)

Table 2.1: Description of artifacts, alloys and corrosion products……... 15
Table 2.2: Representative electron microprobe analyses of tin corrosion phases… 17

CHAPTER III: ROMARCHITE AND AS SOCIATED PHASES AS COMMON CORROSION PRODUCTS ON PEWTER ARTIFACTS

Table 3.1: Archaeological sites from which pewter artifacts were obtained…….26
Table 3.2: Selected microprobe analyses of the *Queen Anne's Revenge* (1718) pewter……..29
Table 3.3: Selected microprobe analyses of the St. Johns Bahamas wreck (~1550) pewter……..30
Table 3.4: Selected microprobe analyses of *La Capitana* (1715) pewter……..32
Table 3.5: Selected microprobe analyses of the *San José* (1733) pewter……..34
Table 3.6: Selected microprobe analyses of Port Royal, Jamaica (1692) pewter…..36
Table 3.7: Selected microprobe analyses of the *Henrietta Marie* (1701) pewter…..37

INTRODUCTION

This thesis consists of three chapters, each written to stand alone as a journal publication or chapter in a book. Because of this, there is some repetition among the chapters, especially in the introductory and concluding material.

Chapter I, The Corrosion Mineralogy of Metal Artifacts from the *Queen Anne's Revenge* (1718), was written with the intent to submit as part of a collection of articles relating to different aspects of study being conducted on artifacts from Blackbeard's *Queen Anne's Revenge*. This book will be edited by Wayne Lusardi of the Underwater Archaeology Branch of the North Carolina Department of Cultural Resources and is expected to be published by the University Press of Florida. The authorship of this article will be: Stacie E. Dunkle, James R. Craig, and Wayne R. Lusardi.

Chapter II, Romarchite and Associated Phases Formed During the Corrosion of Pewter Artifacts from the *Queen Anne's Revenge* (1718), is to be submitted to *Canadian Mineralogist*, the journal in which the first reference to romarchite appears. The authorship will be: Stacie E. Dunkle, James R. Craig, Wayne R. Lusardi, and J. Donald Rimstidt.

Chapter III, Romarchite and Associated Phases as Common Corrosion Products on Pewter Artifacts, will be submitted to an archaeology journal, most likely *Geoarchaeology*. The authorship will be: Stacie E. Dunkle, James R. Craig, and Wayne R. Lusardi.

CHAPTER I

THE CORROSION MINERALOGY OF METAL ARTIFACTS FROM THE *QUEEN ANNE'S REVENGE* (1718)

Abstract

A summary of the metal artifacts from the *Queen Anne's Revenge* (1718) is presented with a preliminary assessment of the corrosion products that have formed on them. The artifacts were buried in sea sediments off the coast of Beaufort, NC for about 280 years. Artifacts made of iron, lead, tin, copper, mercury, gold, and silver were recovered from the site. Only those made of precious metals, gold and silver, were found to have no corrosion products present. Understanding corrosion phases may aid in determining the composition of unknown artifacts, in predicting the survival time of artifacts and provide insight into the processes of metal corrosion in general.

Introduction

A wide variety of metallic artifacts have been recovered from the site of the *Queen Anne's Revenge*, flagship of Blackbeard the pirate that sank in 1718 and is now buried in sediments off the coast of Beaufort, North Carolina (Lusardi 1999; Lawrence and Wilde-Ramsing 2001). The artifacts recovered to date include nails, cannon, ammunition, eating utensils, decorative implements, and more; undoubtedly the variety will increase with additional recovery efforts. The artifacts are constructed of the major metals used at the beginning of the 18th century: iron, base metals (copper, lead, tin, and mercury), and precious metals (gold and silver) (Craig et al. 2001). With the exception of gold (and silver when alloyed with gold), which has remained unaltered, the metals have corroded during their contact with seawater and sediment pore water. Their corrosion products, including oxides, hydroxides, sulfides and hydroxycarbonates, form at the expense of the underlying metallic artifact and therefore are often considered nuisances by archaeologists and are removed for display purposes. However, understanding of these corroded phases may aid in determining the composition of unknown artifacts, provide insight into the survival time of artifacts, and offer insight into the processes of metal corrosion in general. Another benefit of the mineral layer is that it prevents corrosive elements in the surrounding environment from reaching the uncorroded metal, thereby slowing destruction via a process known as passivation. Numerous studies have considered the general effects of corrosion on metallic artifacts and these are well summarized in North (1987) and North and MacLeod (1987). This paper presents a summary of the metal artifacts from the *Queen Anne's Revenge* (1718) including scanning electron microscope images of the corroded surfaces of several of the artifacts. Corrosion phases were preliminarily identified using semi-quantitative chemical analysis.

Iron

The numerous iron artifacts recovered from the *QAR* site include nails (**Figure 1.1**), cannon, grenades, barrel hoops and anchors. These are made of both cast and wrought iron. Many small artifacts have completely corroded beyond identification, leaving behind only a concretion of iron oxides and/or sulfides. The iron nails are relatively well preserved and consist of pure iron with carbon inclusions and a red iron oxide surface coating that we believe to be goethite (FeOOH). A polished cross section

Figure 1.1: Iron nails, varying in length from 1.5 to 4 inches in length, were found attached to a cannon in a large concretion.

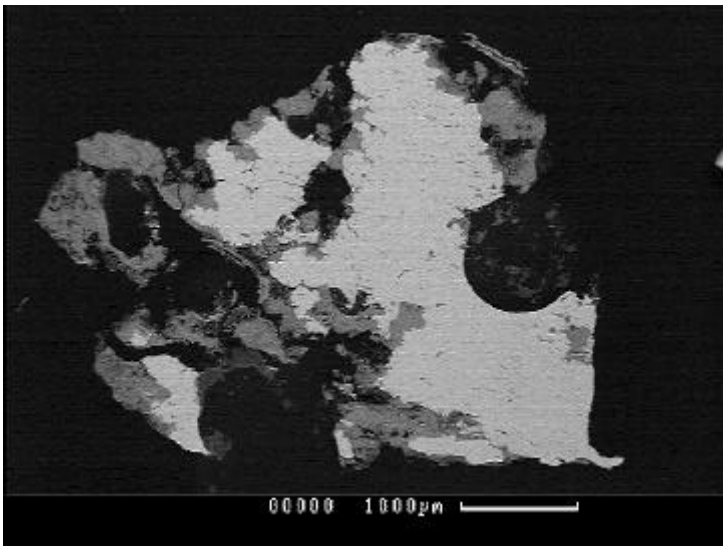

Figure 1.2: Backscattered electron image of a polished cross section of an iron nail. Two phases can be seen, the brighter phase is the uncorroded iron metal while the darker phase on the outside surface of the artifact is an iron oxide, probably goethite (FeOOH).

of one nail is shown in **Figure 1.2**. Iron disulfide, pyrite mixed with marcasite, was observed in some concretions and can be seen as the bright phase along the edge of sand grains in **Figure 1.3**. Iron disulfide was also observed associated with galena (PbS) in a concretion of lead shot. The occurrence of sulfide phases indicates reducing conditions, in which sulfur-reducing bacteria create sulfide ions, are present within some concretion. Concretion formation is characteristic of iron corrosion in seawater and causes the reactions occurring within to be almost completely isolated from outside conditions (North and MacLeod 1987).

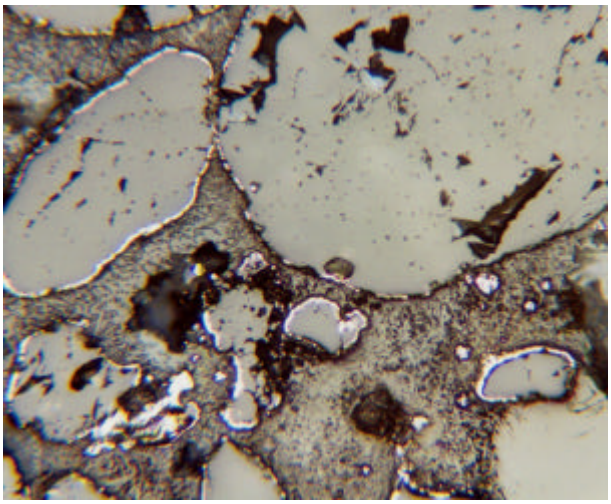

Figure 1.3: Iron disulfide precipitated on the outside surface of quartz sand grains in concretion. This image represents a region about 3 mm wide.

Lead

Many lead artifacts have also been recovered from the wreck site. These include several sizes of shot (**Figure 1.4**), bilge pump sieves, lead stripping, a cannon apron and several weights. A polished cross section of a concretion of bird size lead shot is shown in **Figure 1.5**. The mineral that is cementing this concretion together appears to be hydrocerrusite ($Pb_3(CO_3)_2(OH)_2$). As mentioned previously, galena (PbS) was also observed forming on lead artifacts.

Figure 1.4: Lead shot of various sizes

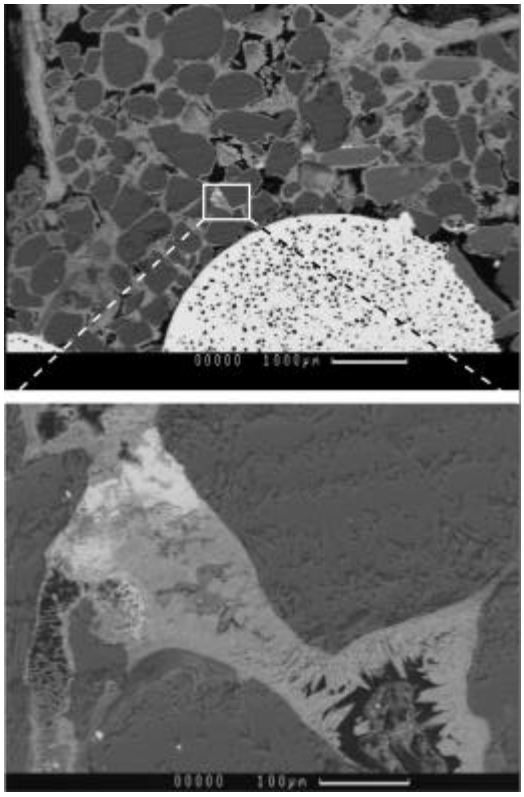

Figure 1.5: Polished cross section of a lead shot concretion. The large dark irregular areas are quartz sand grains cemented within the concretion. The image at higher magnification shows crystals of lead corrosion minerals, probably galena (PbS) (bright phase) and hydrocerrusite ($Pb_3(CO_3)_2(OH)_2$) (medium phase). In the upper image, the small dark irregular areas in the bright, round lead shot are aluminum that became embedded within the soft lead during polishing.

Tin

Most of the tin found on the wreck site is in the form of a pewter alloy, consisting of a matrix of pure tin with copper-rich blebs, ranging from 10-30 microns in their longest dimension, consisting of 25-30 weight percent copper. Subhedral iron and iron arsenide inclusions, most likely the result of impurities in the original tin ore, are also rarely observed within the alloy. Overall, the bulk composition of the pewter is 96 to 98 weight percent tin. Pewter artifacts include several chargers, dishes and plates (**Figure 1.6**), a pewter syringe and a pewter spoon. A tin sulfide, believed to be herzenbergite (SnS), was observed on contents from within the pewter syringe; it apparently formed as the tin reacted with sulfide in this reducing environment. Other tin corrosion phases observed were abhurite ($Sn_3O(OH)_2Cl_2$), romarchite (SnO) and hydroromarchite ($5SnO{\cdot}2H_2O$) that formed on the surfaces of the artifacts corroding in the oxidizing seawater. These phases are shown on a polished cross section of a sampling of a pewter charger in **Figure 1.7.** The nature and distribution of the tin corrosion phases are described in greater detail in Chapters II and III.

Figure 1.6: The recovery of a pewter charger by Wayne Lusardi, curator of the shipwreck project, at the *Queen Anne's Revenge* site.

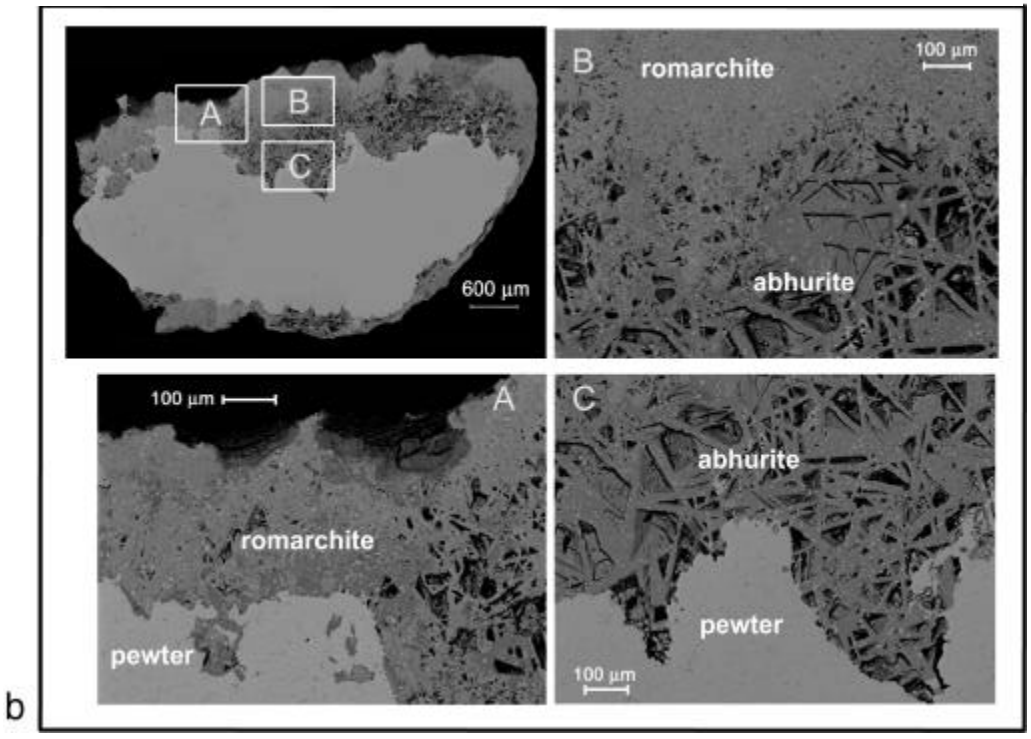

Figure 1.7: Corrosion phases on a polished cross section of a pewter artifact. The boxes (A-C) represent the regions shown at higher magnification in the labeled images.

Copper

Although some copper was observed in pewter artifacts from the *Queen Anne's Revenge* site, more copper-rich artifacts, made of bronze and brass, were also recovered. Most of the scientific and navigational equipment collected from the shipwreck, including a universal staff mount (**Figure 1.8**) and sight, as well as some parts of guns, such as a muskatoon barrel and a side plate, were made of brass, an alloy of copper and zinc. Although the copper and zinc corrosion phases present on the surface of the artifacts were not identified, the copper-oxide cuprite (Cu_2O) is believed to be present (**Figure 1.9**). Several brass pins, possibly used in clothing or furniture, were also collected (**Figure 1.10**). Corrosion phases observed on one of the brass straight pins is seen in **Figure 1.11**.

Figure 1.8: Universal staff mount made of brass

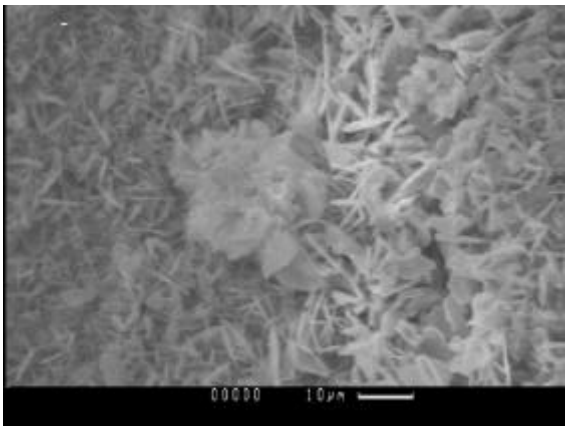

Figure 1.9: Crystals of copper oxide (probably cuprite [Cu_2O]) growing on an unidentified piece of brass

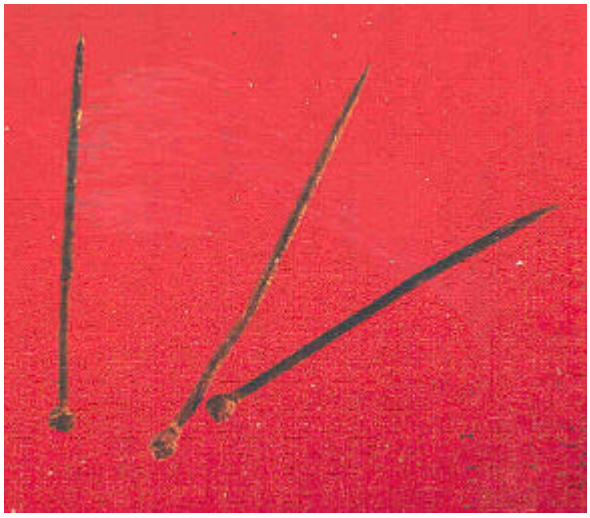

Figure 1.10: Brass straight pins about 2.5 cm in length

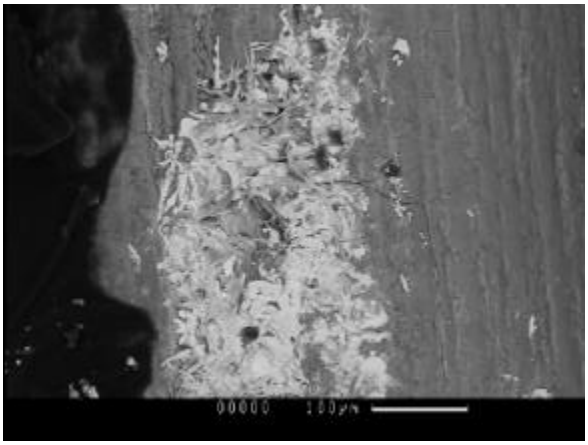

Figure 1.11: Surface of a brass pin showing copper and zinc oxides.

Mercury

A bright red phase, most likely cinnabar (HgS), was observed on contents from within the pewter syringe mentioned previously (**Figure 1.12**). Mercury compounds were used for the treatment of venereal diseases during the 18th century and the cinnabar is most likely the result of the leftover mercury reacting with sulfide in the reducing environment within the pewter syringe.

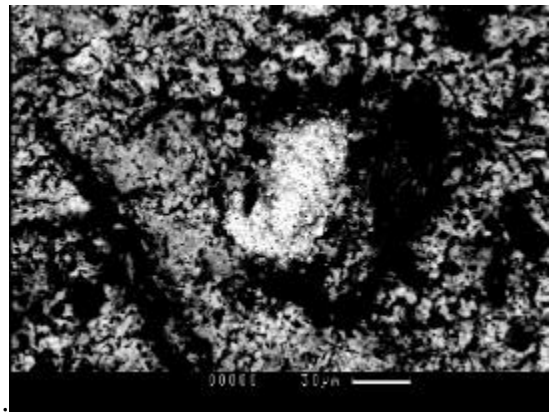

Figure 1.12: Contents from within the pewter syringe demonstrate a bright phase rich in mercury, most likely cinnabar (HgS), surrounded by a tin sulfide

Gold and Silver

Most of the precious metals collected from the wreck site are represented in approximately 100 gold grains ranging from less than 1 to 10 mm in size (**Figure 1.13**). All of the grains are free of any corrosion phase and most consist of a core of gold and silver (10-35%) and a rim of pure gold (**Figure 1.14**). This texture is typical of gold from placer deposits (Craig 2001) but does not present any further clues to the origin of the grains. The only other gold and silver artifact recovered from the wreck site is one small clasp, approximately 1 cm across.

Figure 1.13: Gold grains

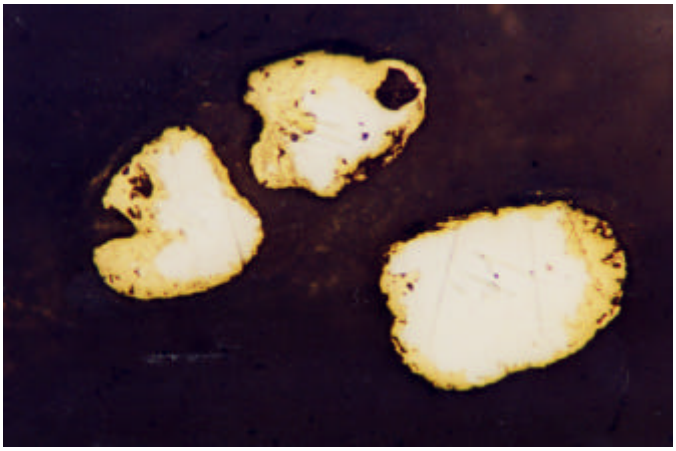

Figure 1.14: Polished cross section of gold placer grains demonstrating pure gold rims and silver rich cores. These grains are approximately 1 mm in diameter.

Table 1.1: Summary of the metal artifacts and their corrosion products found at the wreck site of the *Queen Anne's Revenge* (1718).

Metal	Artifact Type	Corrosion Products
Iron	Nails, Barrel Hoops, Cannon, Anchors, Grenades	Goethite (FeOOH) Pyrite/Marcasite (FeS_2) other iron oxides
Lead	Shot, Cannon Apron, Bilge Pump Sieve, Stripping, Weights	Hydrocerrusite ($Pb_3(CO_3)_2(OH)_2$) Galena (PbS)
Tin	Pewter Chargers, Dishes, Plates, Syringe, Spoon	Abhurite ($Sn_3O(OH)_2Cl_2$) Romarchite (SnO) Hydroromarchite ($5SnO{\cdot}2H_2O$) Herzenbergite (SnS)
Copper	Brass Navigational Equipment, Gun Parts, Straight Pins Bronze Bell	Cuprite (Cu_2O) and other unknown copper oxides
Mercury	Syringe Contents	Cinnabar (HgS)
Gold and Silver	Placer Gold Grains, Decorative Clasp	None

Summary

Most of the metallic artifacts from the *Queen Anne's Revenge* (1718) have suffered some corrosion over time. The phases that form on the surfaces of these artifacts can provide insight into the long-term processes of metal corrosion in seawater that cannot be directly studied in the laboratory. These phases include oxides, hydroxides, sulfides, hydroxycarbonates and more. **Table 1.1** is a summary of the artifacts and the corrosion products observed on them. Iron artifacts are perhaps the most corroded of all the artifacts analyzed, with many of them remaining only as concretions of iron oxides; in local reducing environments, iron disulfide has developed. The lead artifacts have both hydroxycarbonate and sulfide on their surface, depending on the microenvironment of corrosion. Tin artifacts have a significant tin hydroxychloride phase (abhurite [$Sn_3O(OH)_2Cl_2$]) as well as romarchite (SnO) and its hydrous form, hydroromarchite ($5SnO{\cdot}2H_2O$), on their surfaces. The reducing environment inside the pewter syringe led to the formation of tin and mercury sulfide phases. Copper artifacts, most consisting of a brass alloy including zinc, display a surface of platy copper oxides. Gold and silver artifacts show no significant corrosion phase. It should be noted that in addition to the formation of these corrosion products, other minerals have precipitated on the surfaces of these artifacts. Calcium carbonate was observed on the outermost surface of a pewter charger and gypsum crystals were observed within the pewter syringe (**Figure 1.15**). Overall, the surface mineralogy of corroding metals in seawater is quite complex. Archaeological artifacts can serve as models of long-term processes of metal corrosion in a variety of weathering environments.

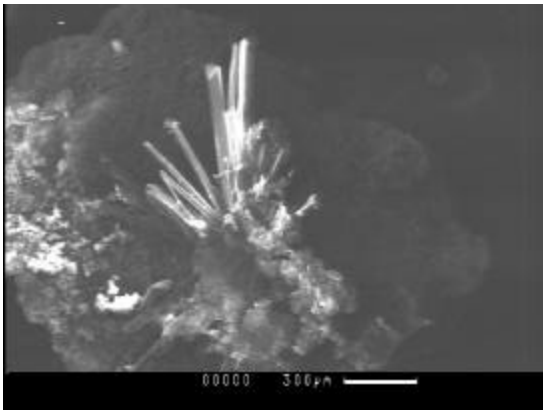

Figure 1.15: Gypsum from within the pewter syringe

CHAPTER II

ROMARCHITE AND ASSOCIATED PHASES FORMED DURING THE CORROSION OF PEWTER ARTIFACTS FROM THE *QUEEN ANNE'S REVENGE* (1718)

Abstract

For the last 400 years, pewter, a tin-rich alloy, has been widely used for ornamental and utilitarian purposes because it is durable, relatively easily worked, resistant to corrosion, and similar to silver in appearance. Pewter plates and implements have been recovered and examined from what is believed to be the wreck site of the *Queen Anne's Revenge*, flagship of the pirate Blackbeard, that sank near Beaufort, North Carolina in 1718. All of the pewter artifacts from the site display a surface veneer of corrosion products and may be viewed as 280 year long experiments of tin corrosion. Mineralogical examination of pewter samples has revealed that the corrosion products are composed of romarchite (SnO), hydroromarchite ($5SnO{\cdot}2H_2O$), and abhurite ($Sn_3O(OH)_2Cl_2$). The romarchite occurs as irregular grains and laths up to 100 microns in length. Thermodynamic considerations reveal that romarchite is most likely a metastable phase, present as the result of sluggish kinetics in the process of the formation of cassiterite (SnO_2), the most stable tin oxide in most natural environments. Observation and identification of these phases will be useful in understanding the stability of tin in the weathering environment and the nature of the metal's corrosion products.

Introduction

For more than 10,000 years, humans have used metals to create both utilitarian and ornamental implements. These implements now provide a rich legacy of artifacts ranging from jewelry to tools and weapons that provide insight into past cultures. Most metallic items suffer some corrosion over time, usually as a result of oxidation by air and/or water. Corrosion is nature's reclamation of the pure metals back into more stable phases that are commonly similar to the ore minerals from which the metals were originally refined. The corrosion phases are often considered nuisances that form at the expense of the underlying metal, destroying or obscuring surface features. Although this may be true, the corrosion phases are extremely beneficial in that they often provide protection, or passivation, for the artifact by forming layers that shield the remaining metal and thus slow destruction. The corrosion layer provides a durable and sometimes impenetrable skin that protects the underlying metal from further interaction with corrosive elements. The corrosion products that form - oxides, hydroxides, carbonates, sulfides and sulfates - depend upon the initial metals present and the environmental conditions under which the artifacts were buried or submerged. Study of corrosion phases is valuable in interpreting the underlying metallic material and environment of corrosion, and may provide valuable information for determining the best means of preservation or restoration of the artifact.

Pewter implements, made of tin-rich alloys, have been used for more than 3,500 years. The earliest pewter artifact, found in a grave, is attributed to the XVIIIth Dynasty

(1580-1350 B.C.E.) of Abydos, Egypt (Hatcher and Barker 1974; Lusardi [forthcoming]). Pewter was found to be durable, relatively easily worked, and resembling silver in appearance; therefore it has been widely used and is often found in archaeological sites. There are a wide diversity of alloys that are considered to fall under the term "pewter," all containing large amounts of tin and varying amounts of lead, copper, antimony, zinc, bismuth or other hardening metals (Hatcher and Barker 1974). Traditionally, the corrosion materials that form on pewter artifacts in seawater were assumed to be the tin-oxide cassiterite (SnO_2) (North 1987), but recent discoveries have contradicted this assumption. Organ and Mandarino (1971) reported the discovery of corrosion phases on a tin pannikan that had remained submerged in fresh water at Boundary Falls, Winnepeg River, Ontario for approximately 150 years. On the basis of x-ray powder diffraction data, compared with those of synthetic SnO and $5SnO{\cdot}2H_2O$, they proposed the mineral names of romarchite and hydroromarchite for the phases they observed. Their report consisted only of a brief abstract and contained no illustrations. Chung, et al (1997) also detected romarchite using x-ray diffraction while studying the phase evolution of pure tin film formation in air and oxygen. They reported that romarchite was the initial tin phase to form by oxidation but that it subsequently transformed into cassiterite. Williams, et al. (1998) reported x-ray diffraction evidence for the presence of romarchite in black surface residue on ancient Chinese bronze mirrors but were unable to provide visual evidence. Matzko, et al (1985) named and described the tin hydroxychloride abhurite

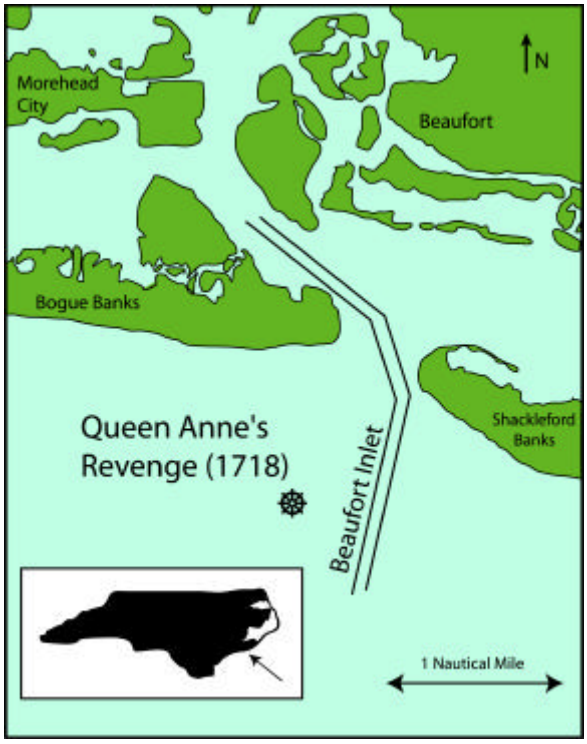

Figure 2.1: Map showing modern location of the *Queen Anne's Revenge*.

($Sn_3O(OH)_2Cl_2$) that had formed on tin ingots submerged in the Red Sea north of Jiddah, Saudi Arabia for about 100 years. They describe the mineral as forming platy, fragile, six-sided crystals averaging 1.5 mm in diameter. Other than these references, romarchite, hydroromarchite and abhurite have remained little known. The only reported pictures of abhurite were by Matzo, et al. (1985) while romarchite and hydroromarchite have never been illustrated in the literature. Hence, the nature and stability of tin corrosion minerals is not well understood; further analysis of pewter archaeological artifacts may provide insight into corrosion processes and prove useful for archaeological conservators.

Scope of Study

This paper is directed toward examining the corrosion of pewter artifacts recovered from the wreck site of *Queen Anne's Revenge*, flagship of the renowned pirate Blackbeard (Lusardi 2000; Lawrence and Wilde-Ramsing 2001). The ship was destroyed by wave action and storms after becoming lodged on a sand bar in Beaufort Inlet, NC in June 1718 (**Figure 2.1**). The wreck was discovered during a magnetometer survey in 1996 after hurricanes Bertha and Fran removed some of the sand covering the remains. Many pewter artifacts have been recovered, including a syringe, a spoon, and a number of chargers, dishes, and plates (**Figure 2.2**) (Craig et al. 2001; Lusardi [forthcoming]).

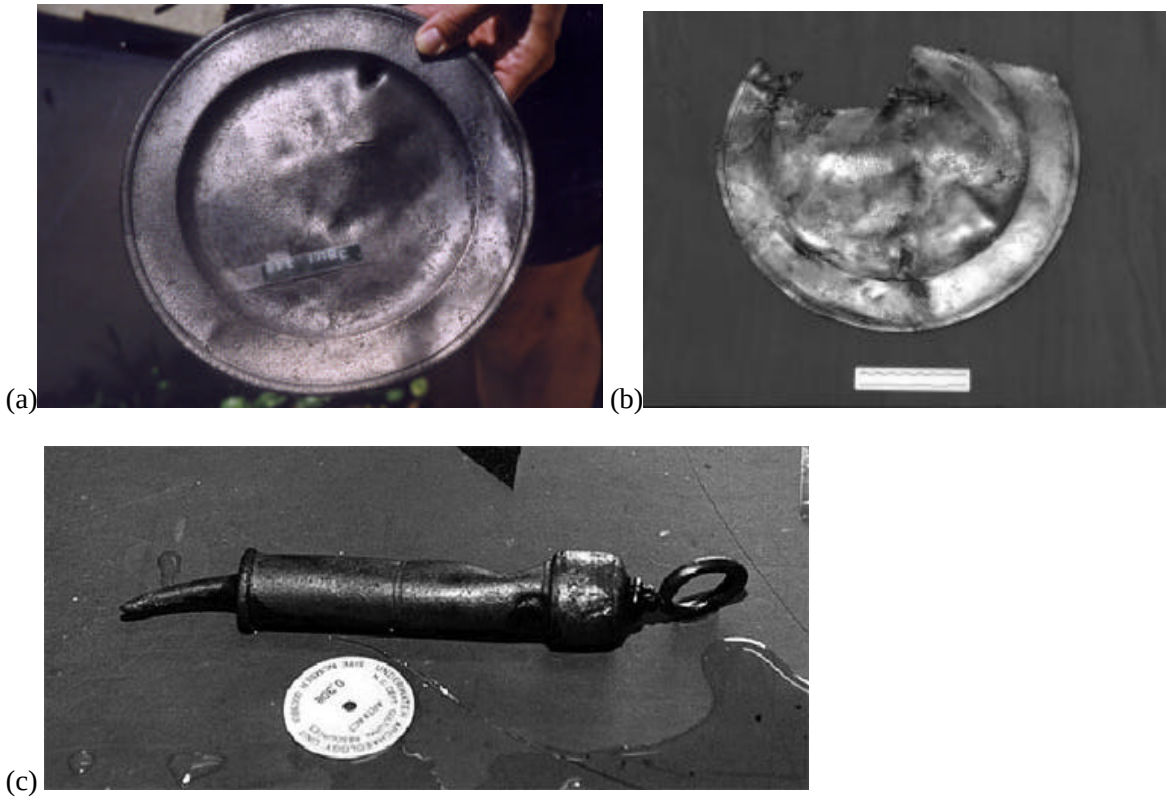

Figure 2.2: Pewter artifacts recovered from the wreck of the *Queen Anne's Revenge*: (a) plate (b) charger and (c) syringe used for the treatment of venereal disease

This study is an analysis of the mineralogy and chemistry of the corrosion products that have formed on the surfaces of these artifacts.

Six samples were examined in this study (**Table 2.1**). The samples were buried in offshore fine sands and silts of coastal North Carolina for approximately 280 years. The corrosion environment varied from oxidizing seawater conditions, as evidenced by the formation of oxides and hydroxides, to sulfur-rich reducing conditions, demonstrated by the presence of sulfide minerals (Craig et al. 2001) and the preservation of organic matter including portions of the ship's wooden hull (Lusardi 2000).

Table 2.1: Description of artifacts, alloys and corrosion products on the six samples.

Artifact Summary			**Microprobe Results**		
Artifact #	Type	Alloying metals	Abhurite	Romarchite	Hydroromarchite
FN-340	plate	Cu, Fe, As	■	■	■
FN-350	charger	Cu, Fe, Pb	■	■	
FN-351	charger	Cu, Fe	■	■	
FN-128	charger	Cu,Fe, As	■	■	■
FN-271	charger	Cu, Fe	no corrosion products were observed*		
FN-457	unknown	Cu, Fe, Pb	■	■	■

*This sample had undergone restoration, which had apparently removed the encrusting corrosion layers.

Sample Analysis

The specimens examined in this study were taken as small but representative fragments (approximately 2 to 5 mm in length) of corroded material from pewter artifacts. The specimens were mounted in a cold setting EPOFIX epoxy; after hardening, these epoxy plugs were ground and polished to expose a cross section of the pewter artifact and corrosion products using methods described in Craig and Vaughan (1994). General textural examination was carried out using standard reflected light microscopy and a Camscan II scanning electron microscope (SEM); backscattered electron images, based upon average atomic weight differences, were found to be particularly useful in deciphering subtle textures. Individual phases were analyzed using a Cameca SX-50 electron microprobe operated at an accelerating voltage of 15.0 keV, a beam current of 20 nA and a beam diameter of 1 μm. These data were used not only to determine the exact chemical makeup of the phases but also to create maps to examine elemental distributions in the uncorroded metal. Limited x-ray powder diffraction data were collected using a Scintag XDS2000 powder diffractometer.

Results

Optical and microprobe analysis of the uncorroded pewter reveals a matrix of pure tin with many small blebs of copper, iron, and iron arsenide (**Figure 2.3**). The copper inclusions are small, relatively high in tin concentration, and much more common than the concentrated inclusions of iron and iron arsenide. The copper inclusions have an irregular shape and are 1 to 30 microns across, while the iron and iron arsenides display subhedral to euhedral crystal forms up to 50 microns long. Trace amounts of lead

were observed in two samples. Spot analyses of these inclusions are presented in **Table 2.2**. Bulk analysis of the pewter artifacts reveals an average composition of 96 to 98 weight percent tin with nearly all of the remainder being copper.

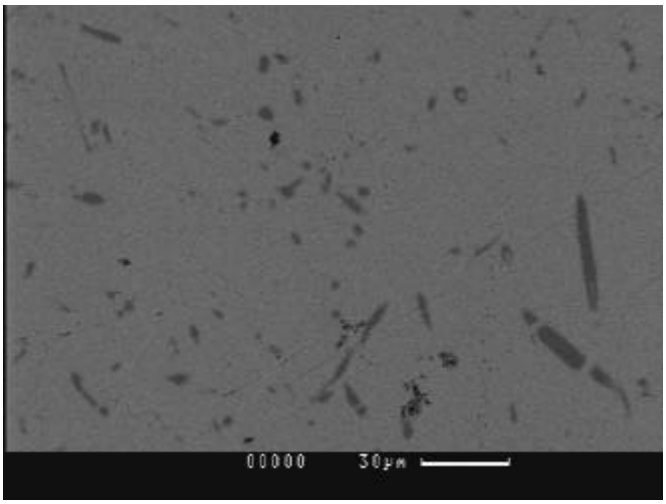

Figure 2.3: Backscattered electron image of a polished surface of pewter from the *Queen Anne's Revenge* 1718 (FN-340). The small, dark irregular blebs are areas of high copper concentration in a matrix of nearly pure tin.

Crystals of tin corrosion minerals can be seen on the surface of most pewter artifacts (**Figure 2.4**). In cross-section, it is apparent that the corrosion of pewter results in the progressive development of enclosing zones of oxide and hydroxide phases as

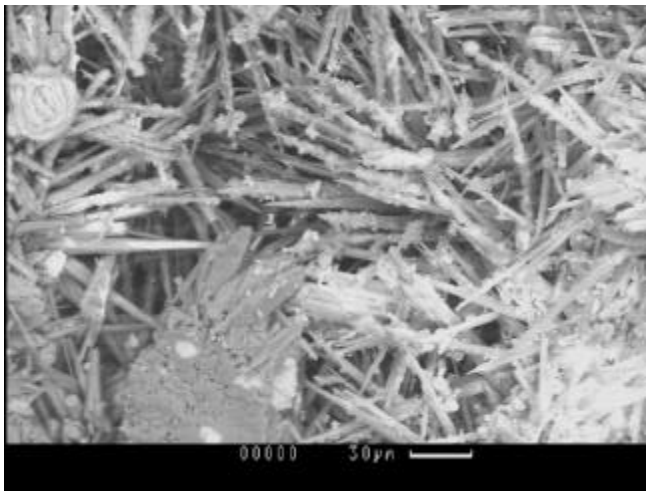

Figure 2.4: Needles of romarchite (SnO) developed on the surface of a pewter charger (FN-350). The crystals are on the outermost surface of the corrosion products, approximately 0.5 mm away from what remains of the original pewter.

Table 2.2: Representative electron microprobe analyses of tin corrosion phases collected using a Cameca SX-50 electron microprobe (reported in weight percent). Ideal elemental weight percents of minerals are shown in italics. The weight percent of oxygen cannot be measured by the electron microprobe and is therefore based upon charge neutrality and the assumed valence of the cations present in the mineral. Also, the ideal weight percent of water is added to the hydrous minerals.

Pewter: Tin matrix

Sn	Cl	As	Cu	Fe	Pb	Total
99.65	0.01	0.01	0.12	0.04	0.19	100.02
98.88	0.01	0.02	0.06	0.00	0.00	98.98
98.78	0.01	0.00	0.13	0.00	0.08	99.01
98.94	0.00	0.00	0.05	0.01	0.00	99.00
98.72	0.01	0.01	0.00	0.02	0.07	98.84
96.95	0.06	0.00	0.23	3.14	0.00	100.36

Pewter: Inclusions in tin matrix

Sn	Cl	As	Cu	Fe	Pb	Total
90.07	0.03	0.02	0.08	12.08	0.02	102.29
83.23	0.01	0.01	0.24	20.04	0.00	103.53
83.52	0.01	0.01	0.19	19.83	0.01	103.57
4.69	0.02	53.56	0.07	42.79	0.00	101.13
1.41	0.01	56.10	0.04	45.95	0.15	103.65
70.81	0.48	0.27	21.43	0.07	0.28	93.33

Abhurite ($Sn_3O(OH)_2Cl_2$)

Sn	Cl	As	Cu	Fe	Pb	O	Semitotal	H_20	Total
74.65	*14.86*	*0.00*	*0.00*	*0.00*	*0.00*	*6.71*	*96.22*	*3.78*	*100.00*
75.16	13.52	0.02	0.25	0.00	0.01	7.15	96.12	*3.78*	99.90
73.53	15.78	0.03	0.04	0.02	0.00	6.38	95.78	*3.78*	99.56
74.67	13.90	0.01	0.07	0.05	0.00	6.96	95.66	*3.78*	99.44
75.26	13.28	0.02	0.09	0.04	0.03	7.19	95.91	*3.78*	99.69
72.64	17.06	0.00	0.00	0.00	0.00	5.94	95.65	*3.78*	99.43
75.08	13.29	0.05	0.03	0.00	0.00	7.15	95.59	*3.78*	99.37

Romarchite (SnO)

Sn	Cl	As	Cu	Fe	Pb	O	Total
88.12	*0.00*	*0.00*	*0.00*	*0.00*	*0.00*	*11.88*	*100.00*
87.59	0.03	0.02	0.08	0.01	0.20	11.85	99.77
88.28	0.16	0.00	0.16	0.00	0.00	11.90	100.50
87.58	0.83	0.01	0.01	0.05	0.09	11.64	100.20
87.47	0.21	0.03	0.09	0.00	0.09	11.78	99.67
87.03	0.21	0.00	0.56	0.00	0.08	11.83	99.71
89.39	0.18	0.00	0.01	0.01	0.00	12.02	101.61
87.80	0.17	0.00	0.14	0.08	0.00	11.86	100.05

Hydroromarchite ($Sn_3O_2(OH)_2$)

Sn	Cl	As	Cu	Fe	Pb	O	Subtotal	H_2O	Total
84.36	*0.00*	*0.00*	*0.00*	*0.00*	*0.00*	*11.37*	*95.73*	*4.27*	*100.00*
82.99	0.41	0.05	1.13	0.05	0.04	11.41	96.09	*4.27*	100.36
84.88	0.52	0.00	0.08	0.03	0.00	11.35	96.86	*4.27*	101.13
84.81	0.27	0.02	0.00	0.24	0.05	11.45	96.83	*4.27*	101.10
84.95	0.39	0.00	0.17	0.05	0.00	11.42	96.97	*4.27*	101.24
82.28	0.27	0.00	0.54	0.05	0.00	11.18	94.32	*4.27*	98.59
85.61	0.22	0.00	0.09	0.00	0.04	11.52	97.47	*4.27*	101.74

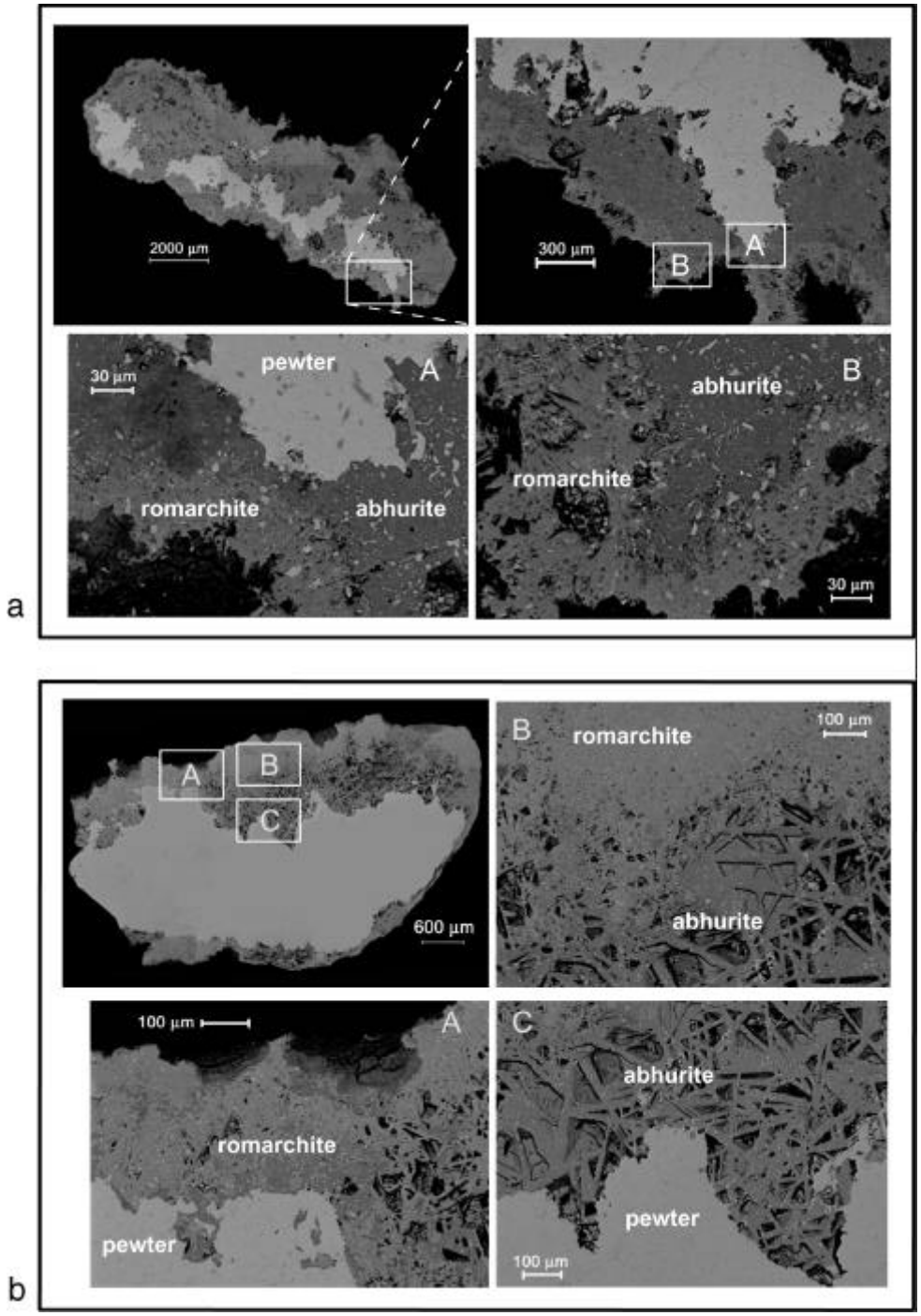

Figure 2.5: Backscattered electron images of corrosion phases on a polished cross sections of pewter artifacts. The boxes are areas represented in other images at higher magnification. (a) FN-457 (b) FN-340

illustrated in **Figure 2.5**. Spot analyses reveal the presence of three tin-oxide corrosion minerals: abhurite ($Sn_3O(OH)_2Cl_2$), romarchite (SnO) and hydroromarchite ($5SnO{\cdot}2H_2O$) (**Table 2.2**). The corrosion occurs in a concentric fashion from the contact with the outside environment to the inner metal. These corrosion layers vary from 10 microns to 2 mm in thickness. Most commonly, the outer layer is made of romarchite and hydroromarchite while the inner corrosion layer is abhurite. The romarchite and hydroromarchite occur as irregular grains or laths up to 100 microns in length. The abhurite occurs in massive layers (**Figure 2.5a**) or in thin plates (**Figure 2.5b**). A tin sulfide mineral, believed to be herzenbergite (SnS), was also observed in material from the shipwreck (**Figure 2.6**) (Craig, et al 2001). This mineral was observed on contents from inside the pewter syringe and most likely formed as the tin reacted with sulfur present as a result of the activities of sulfate-reducing bacteria.

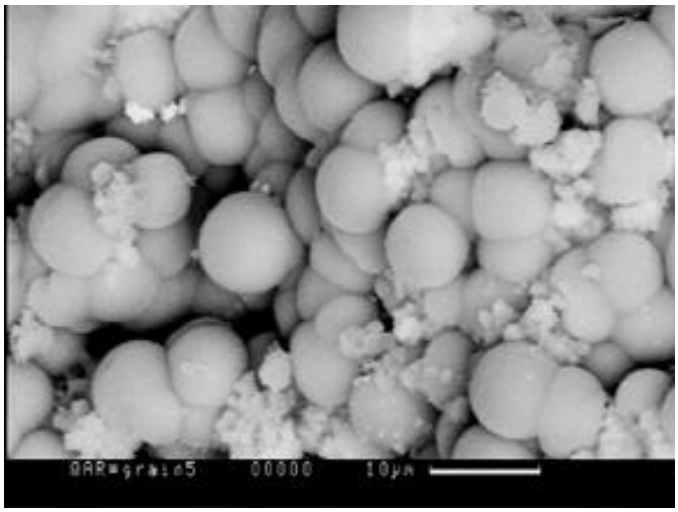

Figure 2.6: Tin sulfide mineral on contents from within the pewter syringe

X-ray diffraction analysis, using Ni-filtered CuKα radiation, was attempted using ground up material from the surface of the pewter artifacts. The observed spacings, in Å, of the reflections (and relative intensities) were: 3.00 (10), 1.80 (3.5), 2.70 (2.7), 1.61 (2) and 1.49 (1.6). These match the data for romarchite reported by Organ and Mandarino (1971).

Discussion

The same corrosion mineralogy formed on all pewter samples regardless of the concentration of copper, iron and iron arsenide within the tin matrix, as long as the artifact was corroding in oxidizing conditions. Because of this, it is believed that romarchite, hydroromarchite and abhurite form universally during tin corrosion in seawater regardless of the composition of the original pewter artifact. Textural analysis using reflected light microscopy and backscattered electron images permits a preliminary assessment to be made concerning the order of formation of tin corrosion minerals

(**Figure 2.5**). Abhurite most often occurs adjacent to the uncorroded metal and still contains metallic tin inclusions within it; therefore it is most likely the first corrosion phase to form in seawater. Over time, the abhurite appears to recrystallize, losing chlorine and recrystallizing as romarchite and hydroromarchite. Cassiterite, previously believed to be the most common tin oxide corrosion mineral, was not unequivocally confirmed on any of the *Queen Anne's Revenge* samples. The absence of cassiterite cannot be explained thermodynamically and therefore may be a result of sluggish kinetics. The stability of tin oxides and dissolved tin species was discussed by Séby, et al. (2001). The Eh/pH conditions present in seawater and marine sediments fall within

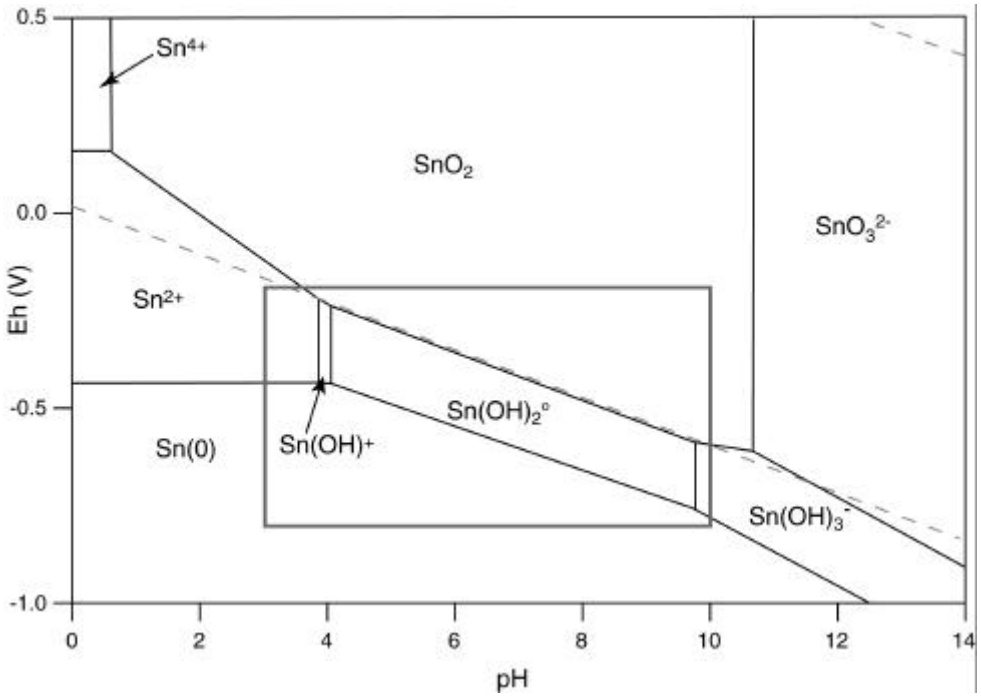

Figure 2.7: The Sn-O-H_2O system at standard state with a dissolved tin activity of 10^{-10} (Séby, et al. 2001). Dashed lines represent the stability field of water. The box represents the area shown in **Figure 2.9**.

the stability field of cassiterite at a dissolved tin activity of 10^{-10} (**Figure 2.7**). Romarchite does not appear on the diagram in **Figure 2.7** because a solution does not become saturated with SnO until a dissolved tin activity of $10^{-6.73}$ is reached at a pH between 4 and 9.7 (**Figure 2.8**). The pH of most seawater is approximately 8.2. **Figure 2.9** illustrates that the $Sn(OH)_2^o$ field shrinks with increased dissolved tin activity at the expense of the growing fields of SnO_2, stable at higher Eh, and Sn(s), stable at lower Eh. Thermodynamic calculations from data presented in Séby, et al (2001) conclude that the Sn(s) field and the SnO_2(s) field converge at an activity of $10^{-6.59}$, suggesting that romarchite is stable over a range of dissolved tin activity from $10^{-6.73}$ to $10^{-6.59}$. It is unlikely that this range is within the error of the data used to make these calculations. Although aqueous tin activity is rarely high enough for romarchite to form in the natural

environment, it is likely that within the pore spaces of a corroding pewter artifact, these activities could occur. Because the stability range of romarchite is so small and the ambient conditions to which the samples were exposed varied with time, it is unlikely that romarchite is a thermodynamically stable phase. However, it is possible to assume

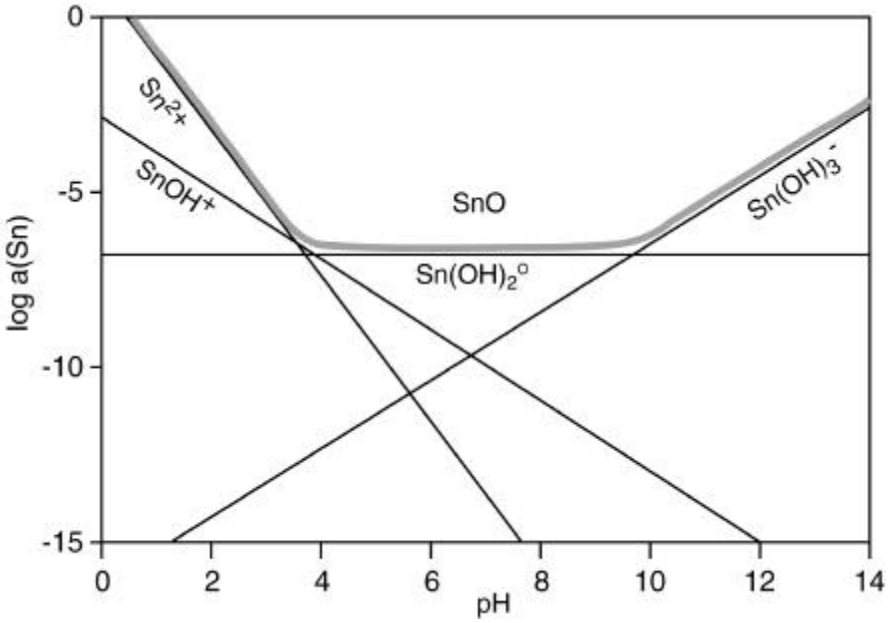

Figure 2.8: Distribution of hydrolysis products in a solution saturated with SnO(s) (Séby, et al. 2001).

that it could form metastably and persist during the 280-year time frame we are considering. If this is true, it is expected that romarchite will eventually recrystallize to form cassiterite. Because romarchite has never been observed in nature other than on corroded tin materials, it is possible that metallic tin is a required precursor for its formation. The near absence of native tin in the natural environment suggests that human intervention may be necessary for the formation of romarchite.

Conclusion

Pewter has been used to construct implements for over 3,500 years and thus provides a rich legacy of archaeological artifacts. Pewter artifacts from the *Queen Anne's Revenge* (1718) provide a 280 year long experiment revealing the metal's reaction to corrosive elements and the nature of the corrosion minerals that result. Although the corrosion phases are normally viewed as a nuisance in the field of archaeology, they actually protect artifacts from further deterioration. Their presence can also provide insight into the processes of tin corrosion that cannot be determined accurately in a normal laboratory time frame. For example, romarchite, little known before this study, has been observed on every pewter artifact from this wreck site if the corrosion products were left intact. In Chapter III this study is expanded to artifacts from five other

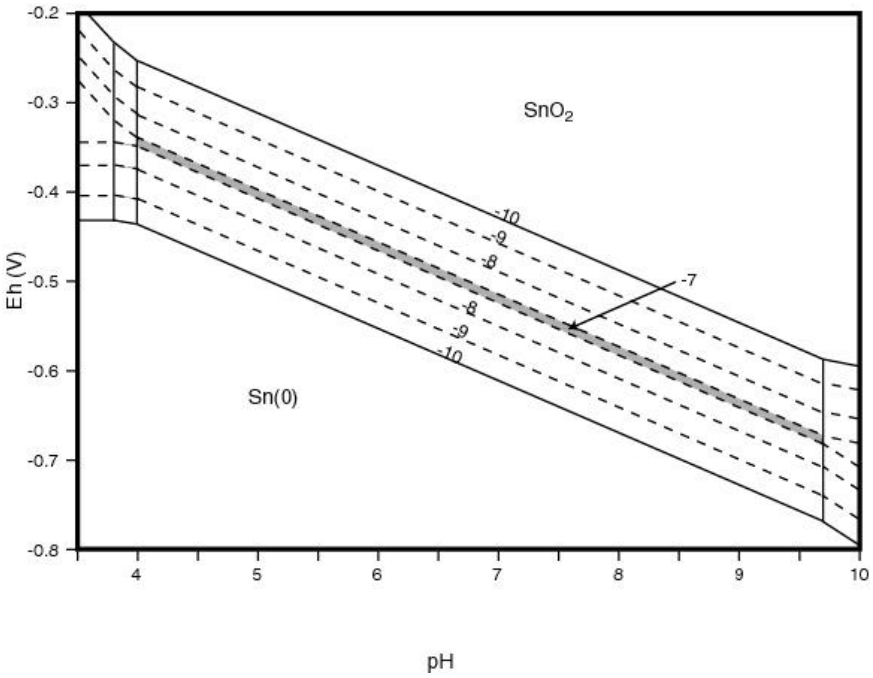

Figure 2.9: Expanded view of $Sn(OH)_2^o$ field from **Figure 2.7** (based on Séby, et al. 2001). The contours represent the log of the aqueous tin activity. The shaded region is the stability field of $Sn(OH)_2^o$ at a dissolved tin activity of 10^{-7}.

submerged archaeological sites on the eastern seaboard of North America and the Caribbean Sea to determine how widespread the occurrence of romarchite is on corroding pewter in seawater. The results suggest that the tin corrosion minerals romarchite, hydroromarchite, and abhurite are much more widespread than has been previously believed. As more is learned about the nature of tin corrosion and metal oxidation in general, the understanding of how these phases serve as a buffer between the reduced metal and the oxidizing natural environment can benefit not only archaeologists in their quest to preserve the physical evidence of our history but may also have wider industrial applications.

CHAPTER III

ROMARCHITE AND ASSOCIATED PHASES AS COMMON CORROSION PRODUCTS ON PEWTER ARTIFACTS

Abstract

Pewter implements have left a legacy of tin-rich artifacts in archaeological sites for more than 3500 years but are most abundant in sites dating to the past 400 years. All of these artifacts have suffered significant alteration over time but the nature of the processes of pewter corrosion and the phases that result has been little understood. Corrosion products were examined from pewter artifacts originating from six different submerged archaeological sites, dating to between ~1550 and 1733, along the eastern seaboard of North America and in the Caribbean Sea. The artifacts were viewed as 270 to 450 year long experiments revealing the phases and mechanisms of tin corrosion in seawater. All of the samples analyzed exhibit abhurite ($Sn_3O(OH)_2Cl_2$), romarchite (SnO), and hydroromarchite ($5SnO{\cdot}2H_2O$) forming at the expense of the underlying artifact. Textural analysis indicates that abhurite is the first alteration product to form, followed by romarchite and hydroromarchite. The corrosion layers on several of the most corroded artifacts also exhibit cassiterite (SnO_2) as a significant and apparently final phase. The absence of this mineral on many samples demonstrates that, while appearing to be stable under the conditions that were present, cassiterite has not yet had time to form. The very limited stability field for romarchite, based on data presented by Séby, et al. (2001), suggests that its presence on these artifacts is the result of a kinetic effect. The universal appearance of this mineral on corroding tin suggests that it is a required step in the oxidation of pure tin to the final most stable phase of cassiterite. Knowledge of the stability of romarchite and its effectiveness as an agent of passivation can provide insight into the formation of tin oxides and the rate of tin corrosion. This can have significant implications from the field of artifact preservation to more widespread industrial applications.

Introduction

The corrosion products that form on metal artifacts after their exposure to the natural environment have commonly been viewed as nuisances to archaeologists because they form at the expense of the underlying metal, destroying or obscuring surface features. Although this is true, the corrosion phases are also extremely beneficial in that they provide protection, or passivation, for the metal by providing a durable and sometimes impenetrable skin that protects the underlying metal from further interaction with corrosive elements. Corrosion is nature's reclamation of the pure metals back into more stable phases that are commonly similar to the ore minerals from which the metals were originally refined. The mineralogical nature of the corrosion products - oxides, hydroxides, carbonates, sulfides and sulfates - varies depending upon the initial metals present and the environmental conditions under which the artifacts have been buried or submerged. Understanding corrosion phases is valuable to archaeologists in interpreting the underlying metallic material and the corrosion environment. It may also provide information valuable in determining the best means of preservation or restoration of the

(a)  (b) 

(c) 

Figure 3.1: Images of pewter artifacts from the wreck site of the *Queen Anne's Revenge* (1718): (a) plate, (b) spoon, and (c) charger being recovered by Wayne Lusardi, the shipwreck project curator.

artifact. By providing long-term models of corrosion that are impossible to reproduce in the laboratory, the study of corroded metal artifacts may have implications beyond the field of archaeology.

Pewter artifacts, made of tin-rich alloys, have been used for ornamental and utilitarian purposes for more than 3,500 years. The earliest pewter artifact, found in a grave, is attributed to the XVIIIth Dynasty (1580-1350 B.C.E.) of Abydos, Egypt (Hatcher and Barker 1974). Pewter was found to be durable, relatively easily worked, and resembling silver in appearance. Because of this, it has been widely used, especially for the last 400 years, and is often found in archaeological sites dating within this time period. Commonly, pewter was used to create plates and chargers for the presentation of food but a large variety of pewter artifacts have been observed, including other eating utensils and medical implements (**Figure 3.1**). A wide diversity of alloys are considered to fall under the term "pewter," all containing large amounts of tin and varying amounts of lead, copper, antimony, zinc, bismuth or other hardening metals (Hatcher and Barker 1974; Lusardi [forthcoming]). Traditionally, the corrosion materials that form on pewter

artifacts were assumed to be the tin-oxide cassiterite (SnO_2) (North 1987) but recent discoveries have contradicted this assumption. Organ and Mandarino (1971) reported the occurrence of SnO and $5SnO{\cdot}2H_20$, which they named romarchite and hydroromarchite respectively, as corrosion phases on a tin pannikan that remained submerged in fresh water at Boundary Falls, Winnepeg River, Ontario for approximately 150 years. Unfortunately, their report consisted only of a brief abstract and contained no illustrations. Chung, et al. (1997) also observed romarchite using x-ray diffraction while studying the phase evolution of a pure tin film in air and oxygen. They reported that romarchite was the initial oxidized tin phase to form but that it subsequently transformed into cassiterite. Williams, et al. (1998) reported x-ray evidence for the presence of romarchite in black surface residue on an ancient Chinese bronze mirror but offered no optical or compositional information. Matzko, et al. (1985) named and described the tin hydroxychloride abhurite ($Sn_3O(OH)_2Cl_2$) that had formed on tin ingots submerged in the Red Sea north of Jiddah, Saudi Arabia for about 100 years. They describe the mineral as forming platy, fragile, six-sided crystals averaging 1.5 mm in diameter. Other than these references, romarchite and abhurite have remained little known. The only published pictures of abhurite were by Matzko, et al. (1985), while romarchite has never been illustrated in the literature. Hence, the nature and stability of tin corrosion minerals is not well understood and further analysis of pewter archaeological artifacts could benefit not only artifact conservators but may also have industrial applications.

Figure 3.2: Map showing locations and dates of archaeological sites providing pewter artifacts for analysis in this study.

Scope of Study

This study is an outgrowth of a detailed analysis of pewter artifacts from the *Queen Anne's Revenge*, flagship of the renowned pirate Blackbeard, which sank off of the coast of Beaufort, NC in 1718 (Lusardi 2000; Lawrence and Wilde-Ramsing 2001). As presented in Chapter II, pewter artifacts from the *Queen Anne's Revenge* were analyzed for their corrosion mineralogy, revealing romarchite, hydroromarchite, and abhurite forming in the corrosion layers of all of the samples. After this discovery, pewter artifacts were obtained from five other archaeological sites to determine how widespread these phases occur as tin corrosion products. All of the archaeological sites are submerged in seawater and are located on the eastern seaboard of North America or in the Caribbean Sea (**Figure 3.2**). While most of the sites are approximately 300 years old, they range from the oldest, the St Johns Bahamas site, ~1550, to the youngest site, the *San José*, a part of the Spanish Fleet that wrecked in Florida in 1733. Information concerning the sites from which samples were obtained is presented in **Table 3.1.**

Table 3.1: Archaeological sites from which pewter artifacts were obtained.

Archaeological Site	Date	Location	Description
Queen Anne's Revenge (31-Cr-314)	1718	Beaufort, NC	Blackbeard the pirate and crew ran aground on a sand bar in Beaufort Inlet
St. Johns Bahamas	~1550	Grand Bahama Island	Early Spanish merchant vessel
La Capitana (8-Ir-15)	1715	Indian River County	Part of the Spanish fleet wrecked on the central eastern coast of Florida
San José (8-Mo-101)	1733	Florida Keys	Part of a Spanish fleet that wrecked in the Florida Keys
Port Royal, Jamaica	1692	Port Royal, Jamaica	An English colony on a sandy peninsula slipped into the ocean during an earthquake
Henrietta Marie	1701	Key West, FL	A slave ship that wrecked just west of Key West after delivering African captives to Jamaica

Sample Analysis

The specimens examined in this study were taken as small but representative fragments (approximately 1 to 10 mm in length) of corroded pewter from identified and unidentified artifacts. The specimens were mounted in a cold setting EPOFIX epoxy; these were then ground and polished to expose a cross section of the artifact using standard methods described in Craig and Vaughan (1994). Textural examination was carried out using standard reflected light microscopy and a Camscan II scanning electron microscope (SEM); backscattered electron imagery was found to be particularly useful in deciphering subtle textures because it is based on the average atomic number of each phase. Quantitative chemical analyses of individual phases were obtained using a Cameca SX-50 electron microprobe operated at an accelerating voltage of 15.0 keV, a beam current of 20 nA, and a beam diameter of 1 μm. These data were used not only to

determine the exact chemical makeup of the phases but also to create maps to examine elemental distributions in the uncorroded metal. For a more detailed description of techniques used in this study see Chapter II.

Results

This study examined typical pewter from six well-documented sites as listed in **Table 3.1** and described below:

Pewter from the *Queen Anne's Revenge* (1718)

The pewter samples from the *QAR* consist of a tin matrix with irregular elongate blebs of copper-tin alloy (**Figure 3.3a**). Microprobe analysis indicates that the weight percent of copper in these inclusions varies from 10-25 while the matrix is pure tin (**Table 3.2**). In addition to the copper-rich blebs are small, rare, euhedral to subhedral crystals of iron and iron arsenide (**Figure 3.3b**). These are up to 50 microns in their longest dimension but are more commonly about 30 microns in length. The source of the iron and arsenic is not known but may have resulted from unintended impurities during the smelting of the original tin ore. Overall, the artifacts display a bulk composition of 96 to 98 weight percent tin with nearly all of the remaining being copper.

(a) 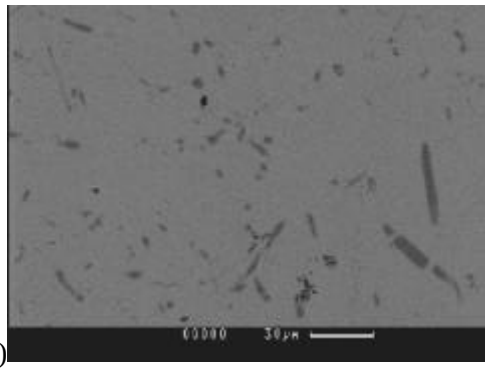 (b) 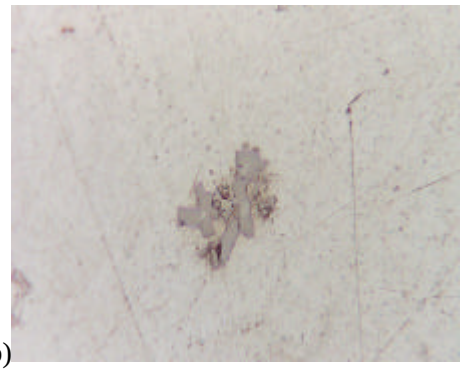

Figure 3.3: Texture of a pewter artifact from the *Queen Anne's Revenge* (1718) with (a) copper-rich blebs in a pure tin matrix (backscattered electron image) and (b) iron-arsenide inclusions in tin/copper matrix.(reflected light image). The region represented in the image is about 300 micron wide.

The corrosion products on the *QAR* pewter samples are about 2-3 mm thick in most regions and typically occur as highly irregular crusts that sometimes deeply embay the underlying pewter. The corrosion phases present are abhurite, romarchite and small amounts of hydroromarchite, as illustrated in **Figure 3.4**. The abhurite occurs both euhedrally and as thin plates and typically contains small residual inclusions of tin and other metals from the original pewter alloy. The romarchite and hydroromarchite occur as laths up to 100 microns in length and are quite intergrown, making them indistinguishable in most images. **Figure 3.5** demonstrates romarchite and

hydroromarchite precipitated on the surface of quartz grains causing them to become cemented to a pewter artifact. Because the abhurite crystals most commonly occur adjacent to the uncorroded pewter and often contain inclusions of residual metal, it can be concluded that this tin hydroxychloride is the first corrosion product to form on pewter artifacts when they are submerged in seawater. The abhurite then appears to lose chloride ions and recrystallize to form romarchite and hydroromarchite.

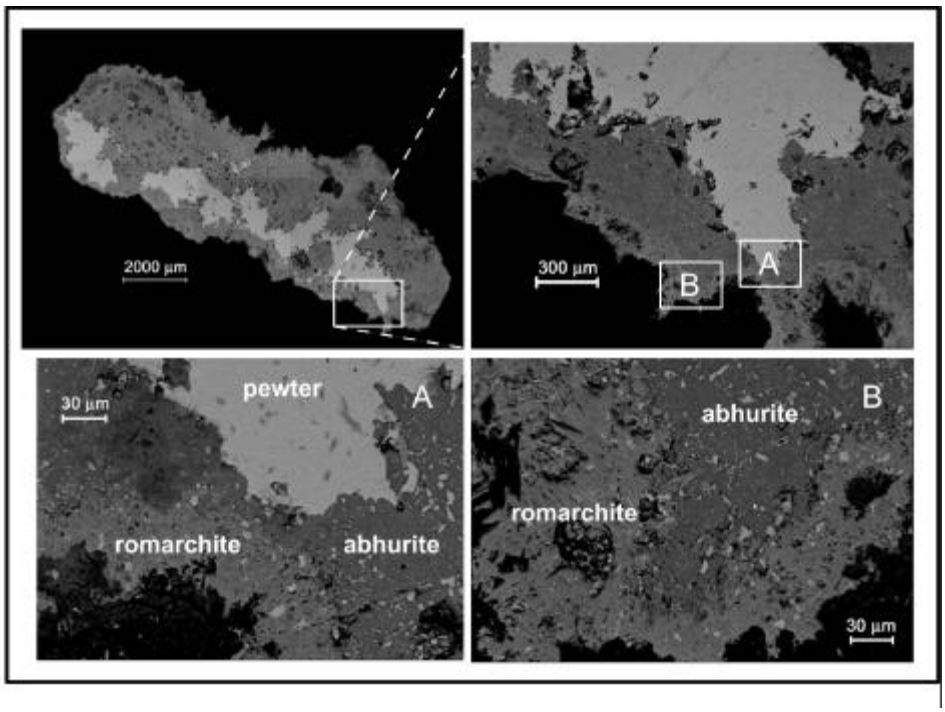

Figure 3.4: Backscattered electron image of a polished cross section of a pewter artifact from the *Queen Anne's Revenge* (1718).

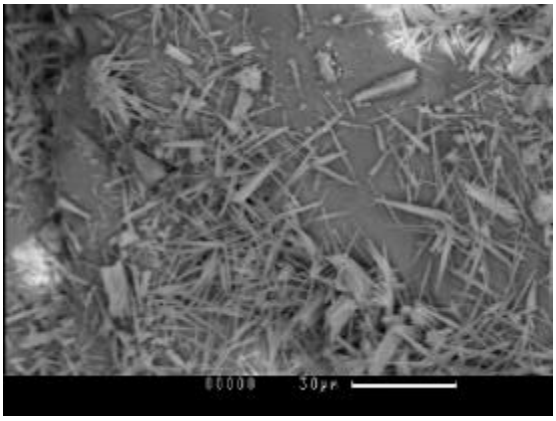

Figure 3.5: SEM photograph of romarchite and hydroromarchite precipitated on quartz sand grains on the surface of a pewter artifact from the *Queen Anne's Revenge* (1718)

Table 3.2: Selected microprobe analyses of the *Queen Anne's Revenge* (1718) pewter and corrosion products collected using a Cameca SX-50 electron microprobe (reported in weight percent). Ideal elemental weight percents of minerals are shown in italics. The weight percent of oxygen cannot be measured by the electron microprobe and is therefore based upon charge neutrality and the assumed valence of the cations present in the mineral. Also, the ideal weight percent of water is added to the hydrous minerals.

Pewter: Tin Matrix

Sn	Cl	As	Cu	Fe	Pb	Total
99.65	0.01	0.01	0.12	0.04	0.19	100.02
98.88	0.01	0.02	0.06	0.00	0.00	98.98
98.78	0.01	0.00	0.13	0.00	0.08	99.01
98.94	0.00	0.00	0.05	0.01	0.00	99.00

Pewter: Metal Inclusions

Sn	Cl	As	Cu	Fe	Pb	Total
4.69	0.02	53.56	0.07	42.79	0.00	101.13
96.95	0.06	0.00	0.23	3.14	0.00	100.36
90.07	0.03	0.02	0.08	12.08	0.02	102.29
92.03	0.00	0.02	1.67	4.61	0.00	98.33

Abhurite ($Sn_3O(OH)_2Cl_2$)

Sn	Cl	As	Cu	Fe	Pb	O	Subtotal	H_20	Total
74.65	*14.86*	*0.00*	*0.00*	*0.00*	*0.00*	*6.71*	*96.22*	*3.78*	*100.00*
72.64	17.06	0.00	0.00	0.00	0.00	5.94	95.65	*3.78*	99.43
70.82	16.81	0.03	0.05	0.00	0.02	7.66	95.40	*3.78*	99.18
75.08	13.29	0.05	0.03	0.00	0.00	7.15	95.59	*3.78*	99.37
74.67	13.90	0.01	0.07	0.05	0.00	6.96	95.66	*3.78*	99.44

Romarchite (SnO)

Sn	Cl	As	Cu	Fe	Pb	O	Total
88.12	*0.00*	*0.00*	*0.00*	*0.00*	*0.00*	*11.88*	*100.00*
87.59	0.03	0.02	0.08	0.01	0.20	11.85	99.77
87.03	0.21	0.00	0.56	0.00	0.08	11.83	99.71
87.58	0.83	0.01	0.01	0.05	0.09	11.64	100.20
87.80	0.17	0.00	0.14	0.08	0.00	11.86	100.05

Hydroromarchite ($Sn_3O_2(OH)_2$)

Sn	Cl	As	Cu	Fe	Pb	O	Subtotal	H_20	Total
84.36	*0.00*	*0.00*	*0.00*	*0.00*	*0.00*	*11.37*	*95.73*	*4.27*	*100.00*
84.81	0.27	0.02	0.00	0.24	0.05	11.45	96.83	*4.27*	101.10
84.88	0.52	0.00	0.08	0.03	0.00	11.35	96.86	*4.27*	101.13
82.99	0.41	0.05	1.13	0.05	0.04	11.41	96.09	*4.27*	100.36

Pewter from the St. Johns Bahamas site (~1550)

Pewter samples from the *St. Johns Bahamas* site consist of a pure tin matrix with copper-rich blebs similar to those present in the *Queen Anne's Revenge* pewter. Although no iron arsenide inclusions are observed, iron inclusions along with several lead rich regions were analyzed (**Table 3.3**). Lead was often added to pewter alloys to make it more malleable but this also led to a decrease in its value. The corrosion layers

on the *St. Johns* pewter are concentric with an especially thick abhurite layer relative to the romarchite/hydroromarchite layer on the outer surface (**Figure 3.6**). Although no specific cassiterite phase could be differentiated in backscattered electron images, microprobe analysis suggests that some cassiterite may be interspersed with the outer layer of romarchite and hydroromarchite. Although this archaeological site is about 150 years older than the other sites analyzed, pewter from *St. Johns* appears to be in the same state of the corrosion process as most of the other pewter artifacts. This observation supports the concept of corrosion passivation, the slowing of the corrosion process once a protective layer has formed on the metal object. This layer serves as a buffer between the artifact and the oxidizing conditions of the external environment.

Table 3.3: Selected microprobe analyses of the St. Johns Bahamas wreck (~1550) pewter and corrosion products. See Table 3.2 for further information.

Pewter: Tin Matrix

Sn	Cl	As	Cu	Fe	Pb	Total
98.54	0.04	0.00	0.28	0.02	0.17	99.05
99.25	0.04	0.00	0.12	0.00	0.18	99.59
98.95	0.09	0.00	0.00	0.00	0.15	99.19

Pewter: Metal Inclusions

Sn	Cl	As	Cu	Fe	Pb	Total
82.15	0.04	0.00	0.00	19.45	0.31	101.96
91.17	0.39	0.00	0.00	10.61	1.11	103.28

Abhurite ($Sn_3O(OH)_2Cl_2$)

Sn	Cl	As	Cu	Fe	Pb	O	Subtotal	H_20	Total
74.65	*14.86*	*0.00*	*0.00*	*0.00*	*0.00*	*6.71*	*96.22*	*3.78*	*100.00*
76.84	9.50	0.00	0.04	0.01	0.04	8.23	94.66	*3.78*	98.44
78.42	11.88	0.00	0.00	0.00	0.00	7.89	98.19	*3.78*	101.97
77.00	9.62	0.00	0.00	0.00	0.00	8.21	94.83	*3.78*	98.61
77.19	10.27	0.00	0.01	0.00	0.00	8.09	95.56	*3.78*	99.34

Romarchite (SnO)

Sn	Cl	As	Cu	Fe	Pb	O	Total
88.12	*0.00*	*0.00*	*0.00*	*0.00*	*0.00*	*11.88*	*100.00*
87.76	0.80	0.07	0.02	0.09	0.25	11.72	100.72
88.62	0.25	0.00	0.01	0.05	0.01	11.91	100.86
87.54	0.27	0.00	0.05	0.00	0.10	11.76	99.72
86.13	0.27	0.04	0.20	0.00	1.12	11.70	99.46

Hydroromarchite ($Sn_3O_2(OH)_2$)

Sn	Cl	As	Cu	Fe	Pb	O	Subtotal	H_20	Total
84.36	*0.00*	*0.00*	*0.00*	*0.00*	*0.00*	*11.37*	*95.73*	*4.27*	*100.00*
83.01	0.19	0.00	0.07	0.00	1.13	11.25	95.65	*4.27*	99.92
83.61	0.26	0.00	0.00	0.00	1.28	11.31	96.46	*4.27*	100.73

Cassiterite (SnO_2)

Sn	Cl	As	Cu	Fe	Pb	O	Total
78.77	*0.00*	*0.00*	*0.00*	*0.00*	*0.00*	*21.23*	*100.00*
77.24	0.16	0.00	0.11	0.03	1.73	21.10	100.37

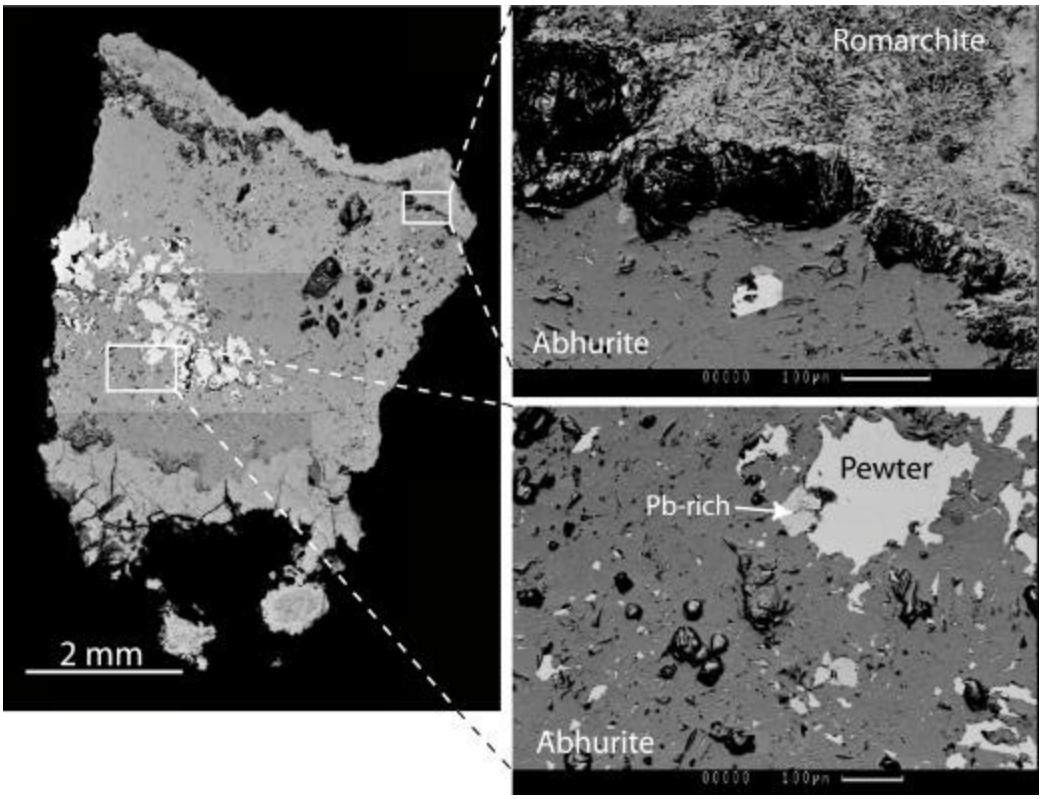

Figure 3.6: Backscattered electron image of a polished cross section of a pewter artifact from the St. Johns Bahamas wreck (~1550)

Pewter from *La Capitana* (1715)

Pewter artifacts recovered from *La Capitana*, the "cabin wreck" of the 1715 Spanish fleet, are some of the furthest along in the corrosion process among those analyzed in this study**.** *La Capitana* pewter consists of a pure tin matrix with copper-rich blebs and rare iron-rich inclusions. The samples demonstrate concentric layers of corrosion products similar to those exhibited by the artifacts from the *Queen Anne's Revenge* and St. Johns; however, the surface of the artifact does not consist entirely of romarchite and hydroromarchite. Instead, these minerals are intergrown with cassiterite in a disorderly fashion (**Table 3.4** and **Figure 3.7**). The texture of the corrosion products in this sample support the previously proposed sequence of corrosion product formation, abhurite then romarchite and hydroromarchite, and suggests that cassiterite is the next phase of the corrosion process. Also, the concentric ordering of corrosion phases is likely a characteristic of artifacts that are less corroded. Cassiterite seems to form in the most porous regions of the corrosion layer. The reason that the pewter from *La Capitana* is further along in the corrosion process than pewter from other sites is unknown but is most likely related to the conditions present in the local burial environment.

Table 3.4: Selected microprobe analyses of *La Capitana* (1715) pewter and corrosion products. See Table 3.2 for further information.

Pewter: Tin Matrix

Sn	Cl	As	Cu	Fe	Pb	Total
98.42	0.24	NA	0.14	0.02	0.08	98.90
98.61	0.27	0.01	0.04	0.07	0.01	98.99
98.10	0.29	0.00	0.18	0.00	0.12	98.69
98.12	0.54	0.00	0.00	0.01	0.06	98.73

Pewter: Metal Inclusions

Sn	Cl	As	Cu	Fe	Pb	Total
66.29	0.51	12.13	24.36	0.02	0.34	103.64
91.17	0.39	0.00	0.00	10.61	1.11	103.28

Abhurite ($Sn_3O(OH)_2Cl_2$)

Sn	Cl	As	Cu	Fe	Pb	O	Subtotal	H_20	Total
74.65	*14.86*	*0.00*	*0.00*	*0.00*	*0.00*	*6.71*	*96.22*	*3.78*	*100.00*
74.42	14.67	NA	0.12	0.02	0.01	8.40	97.65	*3.78*	101.43
74.51	13.59	0.00	0.02	0.01	0.00	6.99	95.11	*3.78*	98.89
72.04	16.69	0.91	0.00	0.01	0.13	6.25	96.04	*3.78*	99.82
73.70	13.57	0.09	0.67	0.04	0.00	7.08	95.15	*3.78*	98.93
67.35	17.02	NA	2.41	0.00	0.00	7.46	94.24	*3.78*	98.02

Romarchite (SnO)

Sn	Cl	As	Cu	Fe	Pb	O	Total
88.12	*0.00*	*0.00*	*0.00*	*0.00*	*0.00*	*11.88*	*100.00*
86.64	0.39	0.03	0.04	0.02	0.19	11.63	98.94
87.96	0.26	0.00	0.07	0.02	0.11	11.83	100.25
86.13	0.27	0.04	0.20	0.00	1.12	11.70	99.46
87.76	0.80	0.07	0.02	0.09	0.25	11.72	100.72

Hydroromarchite ($Sn_3O_2(OH)_2$)

Sn	Cl	As	Cu	Fe	Pb	O	Subtotal	H_20	Total
84.36	*0.00*	*0.00*	*0.00*	*0.00*	*0.00*	*11.37*	*95.73*	*4.27*	*100.00*
84.39	0.57	0.00	0.15	0.00	0.35	11.31	96.78	*4.27*	101.05
83.42	0.57	0.00	0.02	0.00	0.77	11.18	95.96	*4.27*	100.23
84.60	0.30	0.01	0.07	0.04	0.40	11.40	96.81	*4.27*	101.08
83.02	0.44	NA	0.03	0.02	0.37	11.18	95.07	*4.27*	99.34

Cassiterite (SnO_2)

Sn	Cl	As	Cu	Fe	Pb	O	Total
78.77	*0.00*	*0.00*	*0.00*	*0.00*	*0.00*	*21.23*	*100.00*
75.50	0.07	0.58	1.31	0.03	0.01	21.37	98.86
77.97	0.73	0.02	0.25	0.05	0.00	20.86	99.88
77.54	0.35	0.00	0.47	0.00	1.18	21.17	100.71
77.39	0.24	0.00	0.03	0.02	1.64	21.03	100.35

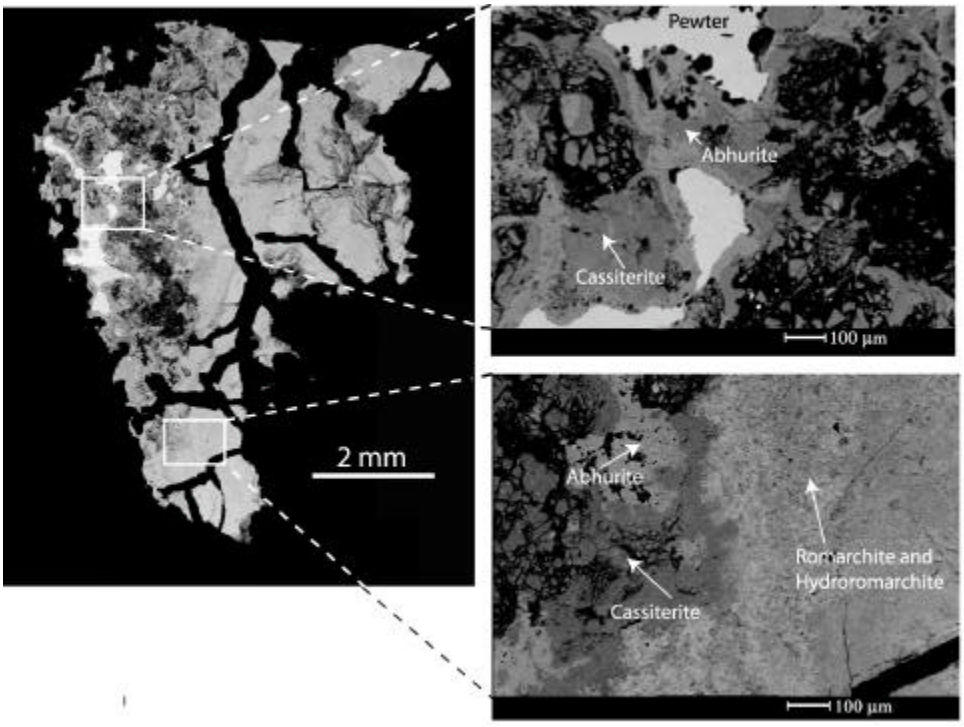

Figure 3.7: Backscattered electron image of a polished cross section of a pewter artifact from *La Capitana* (1715).

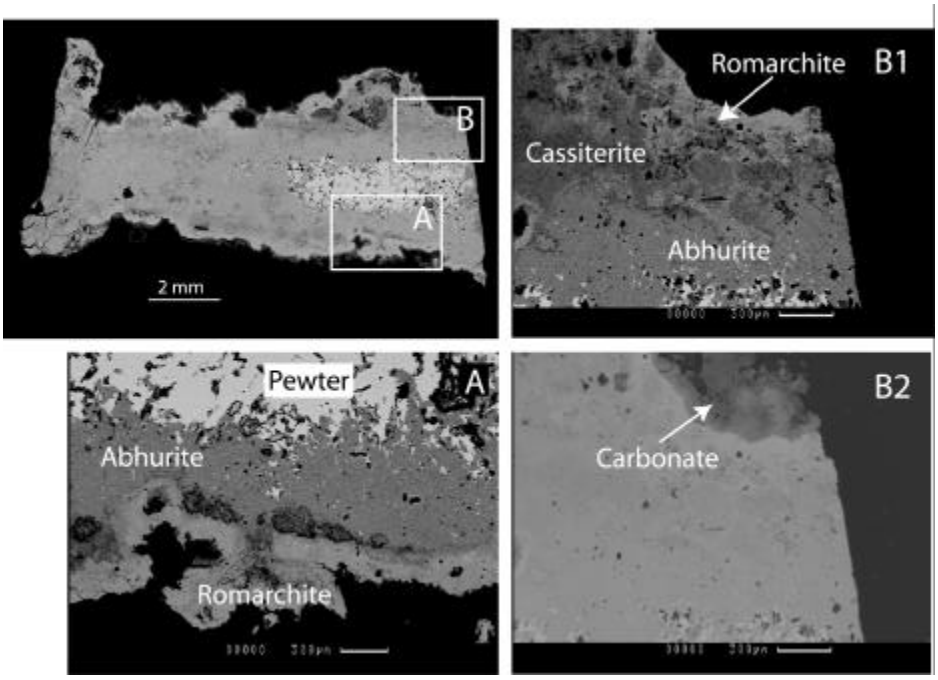

Figure 3.8: Backscattered electron image of a polished cross section of a pewter artifact from the *San José* (1733). Boxes represent regions shown at higher magnification. B2 was taken at a lower contrast than B1 and shows an outer carbonate layer not visible in the other images.

Pewter from the *San José* (1733)

The *San José* pewter also exhibits a pure tin matrix filled with many copper rich blebs. However, unlike the other pewters, instead of iron rich inclusions it contains several arsenic rich zones. Like the pewter from *La Capitana* (1715), this artifact

Table 3.5: Selected microprobe analyses of the *San José* (1733) pewter and corrosion products. See Table 3.2 for further information.

Pewter: Tin Matrix

Sn	Cl	As	Cu	Fe	Pb	Total
98.95	0.02	0.25	0.19	0.00	0.04	99.45
99.45	0.78	0.08	0.20	0.00	0.04	100.55
99.18	0.02	0.10	0.00	0.03	0.03	99.36

Pewter: Metal Inclusions

Sn	Cl	As	Cu	Fe	Pb	Total
95.52	0.02	0.13	3.22	0.04	0.04	98.97
73.63	0.01	28.61	1.83	0.01	0.54	104.63
72.39	0.02	29.27	0.54	0.14	0.00	102.36

Abhurite ($Sn_3O(OH)_2Cl_2$)

Sn	Cl	As	Cu	Fe	Pb	O	Subtotal	H_20	Total
74.65	*14.86*	*0.00*	*0.00*	*0.00*	*0.00*	*6.71*	*96.22*	*3.78*	*100.00*
74.58	12.68	1.00	0.06	0.02	0.05	7.54	95.93	*3.78*	99.71
74.33	14.80	0.41	0.04	0.00	0.22	6.84	96.63	*3.78*	100.41
72.00	17.61	0.28	0.12	0.00	0.00	5.85	95.88	*3.78*	99.66
73.94	16.33	0.08	0.07	0.03	0.09	6.34	96.87	*3.78*	100.65

Romarchite (SnO)

Sn	Cl	As	Cu	Fe	Pb	O	Total
88.12	*0.00*	*0.00*	*0.00*	*0.00*	*0.00*	*11.88*	*100.00*
87.22	0.54	0.02	0.00	0.02	0.91	11.72	100.42
87.49	0.25	0.00	0.06	0.00	0.28	11.77	99.84
87.12	0.19	0.00	0.05	0.00	0.42	11.75	99.52
87.78	0.39	0.02	0.14	0.00	0.76	11.85	100.94

Hydroromarchite ($Sn_3O_2(OH)_2$)

Sn	Cl	As	Cu	Fe	Pb	O	Subtotal	H_20	Total
84.36	*0.00*	*0.00*	*0.00*	*0.00*	*0.00*	*11.37*	*95.73*	*4.27*	*100.00*
83.88	0.43	0.00	0.16	0.00	0.23	11.27	95.97	*4.27*	100.24
83.25	0.45	0.01	0.01	0.02	0.26	11.15	95.15	*4.27*	99.42
83.16	0.32	0.00	0.00	0.00	0.55	11.18	95.21	*4.27*	99.48

Cassiterite (SnO_2)

Sn	Cl	Ca	Cu	Fe	Pb	S	O	Total
78.77	*0.00*	*0.00*	*0.00*	*0.00*	*0.00*	*0.00*	*21.23*	*100.00*
77.61	0.02	0.10	0.04	0.46	0.05	0.13	21.23	99.64
77.16	0.01	0.19	0.03	0.60	0.00	0.07	21.12	99.18
77.62	0.02	0.12	0.09	0.44	0.00	0.07	21.19	99.56
77.86	0.09	0.00	0.00	0.02	0.00	0.16	21.13	99.26

demonstrates what we believe is the entire sequence of phases involved in tin corrosion (**Table 3.5**). **Figure 3.8** shows a layer of abhurite on all sides of the corroding metal while a thin layer of romarchite and hydroromarchite coat the outside of the artifact, except for a carbonate layer seen on the outermost edge of some regions. The cassiterite in this sample appears to be forming in a vesicle most likely created by the breakdown of the earlier formed corrosion minerals. Another pewter artifact from this wreck site demonstrates the presence of iron oxide (probably goethite). The low concentration of iron in the original pewter alloy suggests that the iron oxide formed as the result of the sample being near a corroding iron artifact on the wreck site.

Pewter from Port Royal, Jamaica (1692)

Pewter from Port Royal, Jamaica resembles the pewter from the *Queen Anne's Revenge* quite closely in that it consists of a pure tin matrix, copper-rich blebs and rare inclusions of iron and iron arsenide (**Table 3.6**). This sample, however, also contains lead-rich regions. A cross section of the edge of a corroding pewter artifact, presented in **Figure 3.9**, demonstrates how the abhurite appears to be growing along zones of weakness and pores in the original pewter alloy. Notice also how the precipitation of romarchite and hydroromarchite on the outer edge of the artifact has led to the cementing of quartz sand grains to the object, perhaps further slowing the corrosion process.

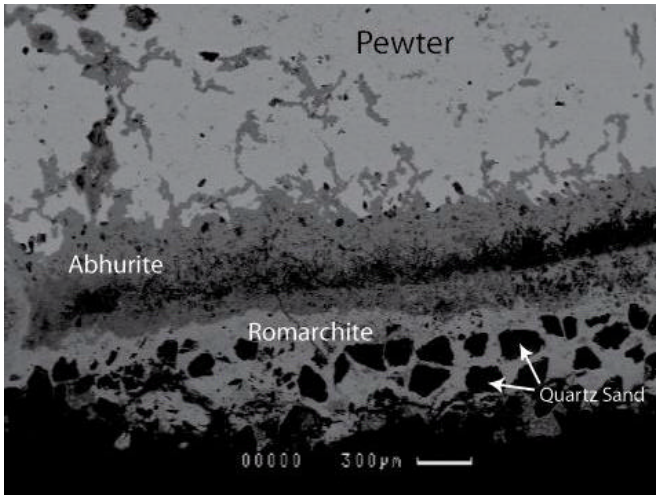

Figure 3.9: Backscattered electron image of a polished cross section of a pewter artifact from Port Royal, Jamaica (1692).

Pewter from the *Henrietta Marie* (1701)

The pewter from the *Henrietta Marie* is the most intensely corroded of all the samples analyzed. The alloy itself is identical to some seen before*:* copper-rich blebs and rare iron and iron arsenide inclusions. The only minor difference is that some of the copper-rich blebs reach nearly 40 weight percent copper (**Table 3.7**). All of the tin oxide phases discussed in previous sections are present on this sample, although the uncorroded metal and abhurite phases are not shown in **Figure 3.10.** This image does, however,

Table 3.6: Selected microprobe analyses of Port Royal, Jamaica (1692) pewter and corrosion products. See Table 3.2 for further information.

Pewter: Tin Matrix

Sn	Cl	As	Cu	Fe	Pb	Total
99.43	0.00	0.01	0.10	0.00	0.27	99.81
99.75	0.09	0.00	0.00	0.01	0.10	99.95
99.45	0.06	0.00	0.11	0.07	0.01	99.70

Pewter: Metal Inclusions

Sn	Cl	As	Cu	Fe	Pb	Total
96.57	0.01	2.55	1.52	0.00	0.34	100.98
5.11	0.00	0.00	0.47	0.00	93.72	99.30
64.27	0.01	0.02	39.10	0.12	0.07	103.59
90.66	0.12	0.04	8.90	0.37	0.04	100.12
2.76	0.01	53.07	0.00	44.72	0.05	100.62
83.32	0.00	0.03	0.04	20.73	0.07	104.19

Abhurite ($Sn_3O(OH)_2Cl_2$)

Sn	Cl	As	Cu	Fe	Pb	O	Subtotal	H_20	Total
74.65	*14.86*	*0.00*	*0.00*	*0.00*	*0.00*	*6.71*	*96.22*	*3.78*	*100.00*
74.08	14.61	0.00	0.04	0.03	0.00	6.71	95.47	*3.78*	99.25
73.96	16.16	0.00	0.00	0.01	0.18	6.34	96.65	*3.78*	100.43
74.90	14.36	0.02	0.02	0.00	0.00	6.87	96.16	*3.78*	99.94
74.01	16.26	0.02	0.00	0.00	0.06	6.32	96.66	*3.78*	100.44

Romarchite (SnO)

Sn	Cl	As	Cu	Fe	Pb	O	Total
88.12	*0.00*	*0.00*	*0.00*	*0.00*	*0.00*	*11.88*	*100.00*
87.85	0.41	0.03	0.00	0.02	0.08	11.77	100.16
88.26	0.24	0.00	0.07	0.00	0.00	11.86	100.43
87.79	0.26	0.01	0.06	0.00	0.06	11.80	99.98
87.38	0.29	0.01	0.00	0.03	0.10	11.93	99.74

Hydroromarchite ($Sn_3O_2(OH)_2$)

Sn	Cl	As	Cu	Fe	Pb	O	Subtotal	H_20	Total
84.36	*0.00*	*0.00*	*0.00*	*0.00*	*0.00*	*11.37*	*95.73*	*4.27*	*100.00*
84.54	0.31	0.02	0.14	0.00	0.92	11.41	97.34	*4.27*	101.61
83.49	0.35	0.03	0.00	0.03	0.07	11.20	95.17	*4.27*	99.44
84.86	0.97	0.00	0.03	0.00	0.08	11.23	97.17	*4.27*	101.44

Table 3.7: Selected microprobe analyses of the *Henrietta Marie* (1701) pewter and corrosion products. See Table 3.2 for further information.

Pewter: Tin Matrix

Sn	Cl	As	Cu	Fe	Pb	Total
99.41	0.01	0.00	1.01	0.02	0.00	100.45
100.09	0.00	0.00	0.17	0.00	0.03	100.30
100.55	0.00	0.00	0.12	0.00	0.10	100.77

Pewter: Metal Inclusions

Sn	Cl	As	Cu	Fe	Pb	Total
63.88	0.01	0.00	36.35	0.68	0.05	100.98
83.21	0.00	0.00	0.10	20.60	0.08	103.99
4.54	0.02	52.88	0.69	45.87	0.00	104.00
77.21	0.04	0.02	24.44	0.05	0.00	101.76
86.73	0.00	0.00	0.86	16.97	0.02	104.59

Abhurite ($Sn_3O(OH)_2Cl_2$)

Sn	Cl	As	Cu	Fe	Pb	O	Subtotal	H_20	Total
74.65	*14.86*	*0.00*	*0.00*	*0.00*	*0.00*	*6.71*	*96.22*	*3.78*	*100.00*
71.45	20.28	0.22	0.00	0.07	0.04	5.15	97.21	*3.78*	100.99
71.28	20.82	0.03	0.00	0.00	0.01	4.92	97.04	*3.78*	100.82
70.74	20.41	0.08	0.00	0.05	0.05	4.97	96.30	*3.78*	100.08
71.44	19.74	0.00	0.23	0.00	0.05	5.24	96.69	*3.78*	100.47

Romarchite (SnO)

Sn	Cl	As	Cu	Fe	Pb	O	Total
88.12	*0.00*	*0.00*	*0.00*	*0.00*	*0.00*	*11.88*	*100.00*
87.89	0.00	0.00	0.48	0.00	0.08	11.97	100.42
87.84	0.26	0.00	0.00	0.03	0.00	11.79	99.92
87.63	0.12	0.01	0.12	0.00	0.03	11.82	99.74
87.91	0.19	0.05	0.31	0.01	0.00	11.91	100.38

Hydroromarchite ($Sn_3O_2(OH)_2$)

Sn	Cl	As	Cu	Fe	Pb	O	Subtotal	H_20	Total
84.36	*0.00*	*0.00*	*0.00*	*0.00*	*0.00*	*11.37*	*95.73*	*4.27*	*100.00*
83.73	0.12	0.00	0.02	0.00	0.09	11.27	95.23	*4.27*	99.50
82.75	0.32	0.12	0.94	0.05	0.00	11.37	95.55	*4.27*	99.82
83.55	0.22	0.12	0.28	0.00	0.00	11.32	95.50	*4.27*	99.77
84.28	0.21	0.00	0.20	0.00	0.00	11.36	96.06	*4.27*	100.33

Cassiterite (SnO_2)

Sn	Cl	As	Cu	Fe	Pb	O	Total
78.77	*0.00*	*0.00*	*0.00*	*0.00*	*0.00*	*21.23*	*100.00*
77.73	0.20	0.14	1.07	0.26	0.07	21.65	101.12
78.45	0.06	0.22	0.84	0.15	0.00	21.77	101.48
75.92	0.09	0.07	0.34	0.79	0.43	21.17	98.81
78.40	0.06	0.01	0.21	0.02	0.05	21.24	99.99

show the laths typical of romarchite and hydroromarchite in polished cross section. As in the case of *La Capitana* pewter, the concentric corrosion layers appear to break down as the corrosion process reaches the last stage of tin oxidation and the romarchite and hydroromarchite recrystallize to cassiterite in a disorderly manner, seemingly in the most porous region of the corrosion layer.

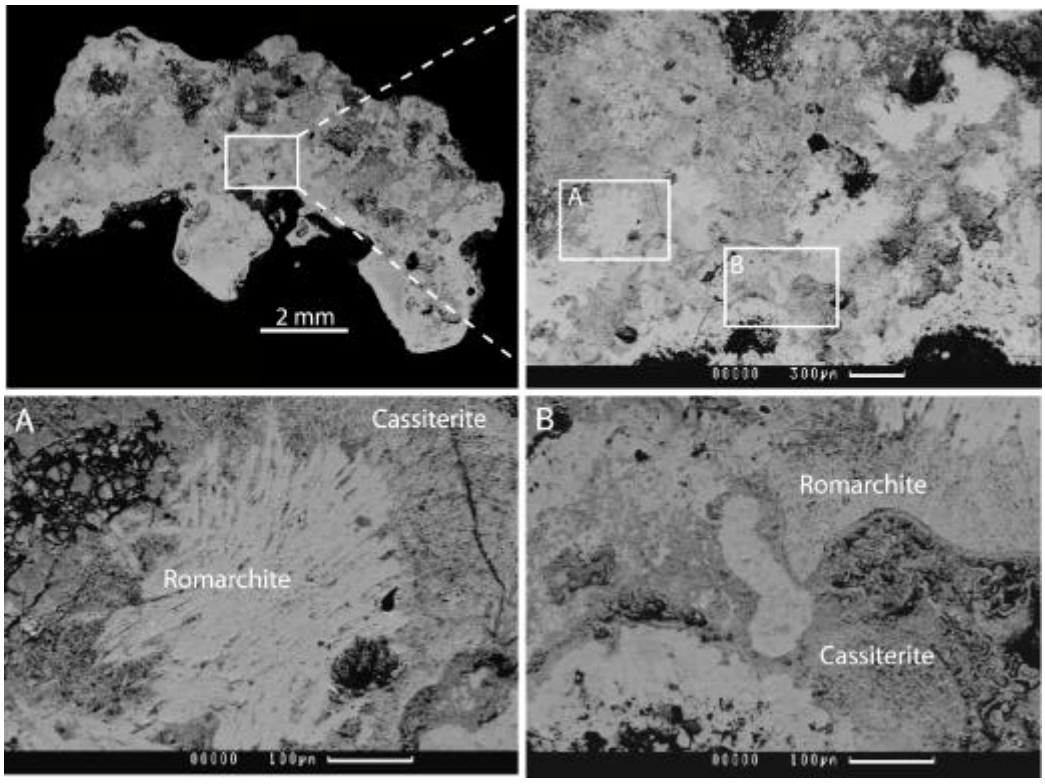

Figure 3.10: Backscattered electron image of a polished cross section of a pewter artifact from the *Henrietta Marie* (1701).

Discussion

The examination of corroded pewter artifacts from six archaeological sites spanning ~180 years (from ~1550 to 1733) reveals a common corrosion mineralogy of abhurite, romarchite and hydroromarchite; cassiterite was also a significant phase forming on some of the artifacts. The presence of romarchite on these artifacts confirms previously unsubstantiated suggestions that the mineral is present as part of the "pustules" that form on corroding pewter artifacts (North 1987). The pewter alloys used to make the artifacts were quite similar, all of them consisting of a pure tin matrix with copper-rich blebs ranging from 10 to 40 weight percent copper. The artifacts also each contained all or some of the following impurities: lead, iron and/or arsenic. Overall, each of the artifacts had a bulk composition of about 96 to 98 weight percent tin. The results of this study suggest that abhurite, romarchite and hydroromarchite form as principal

corrosion products on tin-rich alloys corroding in the marine environment. Textural analysis of the corrosion products on these artifacts, which were submerged for 270-450 years, suggests that abhurite, a tin hydroxychloride, is the first product of tin corrosion in seawater. This is supported by the presence of residual inclusions of metal within an abhurite matrix and the consistent presence of abhurite adjacent to the uncorroded metal. Over time the abhurite appears to recrystallize with loss of chlorine to form romarchite and hydroromarchite. Cassiterite seems to be the final product of tin corrosion as it is present on the artifacts that are most mature in the corrosion process. Although some artifacts are more deeply corroded than others; the depth of corrosion appears to be unrelated to the age of the archaeological site. The degree to which the pewter artifact is corroded probably depends on the oxidizing conditions of the shipwreck location or the microenvironment of the artifact itself.

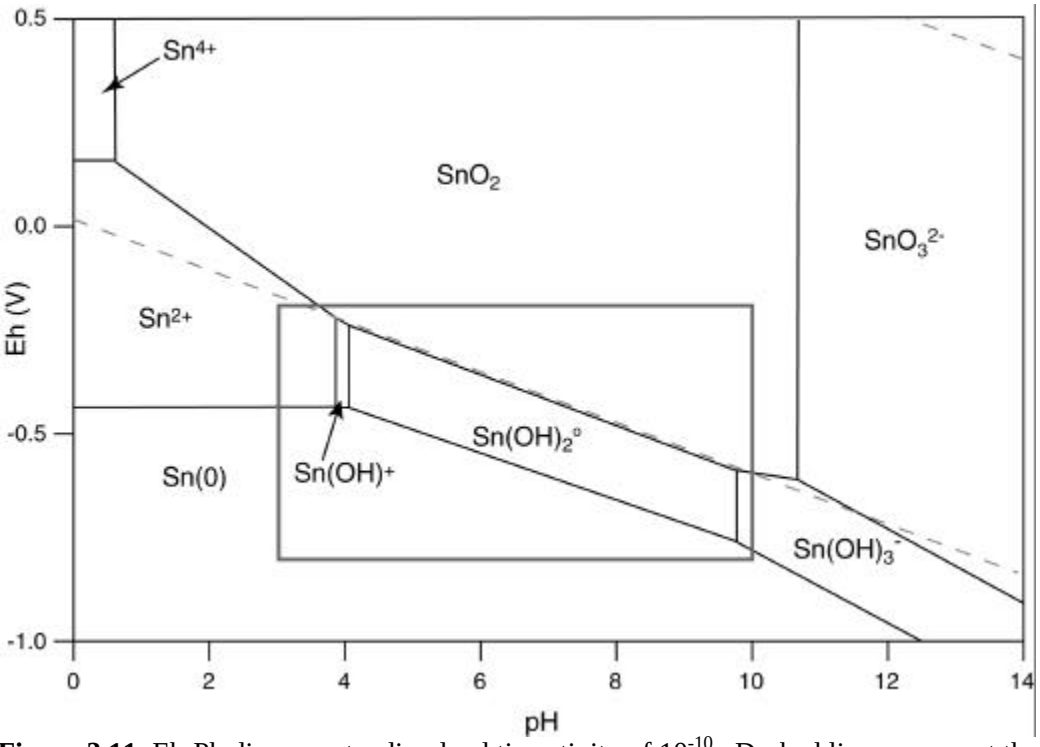

Figure 3.11: Eh-Ph diagram at a dissolved tin activity of 10^{-10}. Dashed lines represent the stability field of water. The box represents the area shown in Figure 3.13. (Séby, et al., 2001)

This sequence of corrosion phases is not only supported by textural analysis of the artifacts but also by thermodynamic and kinetic considerations. As the tin becomes oxidized from its metallic form it loses two electrons causing it to change to Sn^{2+}, the oxidation state of tin in abhurite, romarchite and hydroromarchite. As further oxidation occurs, two more electrons are lost and the tin becomes Sn^{4+}, the oxidation state of tin in cassiterite. The stability of tin oxides and dissolved tin species was discussed by Séby, et al. (2001). The Eh/pH conditions present in seawater and marine sediments fall within the stability field of cassiterite at a dissolved tin activity of 10^{-10} (**Figure 3.11**).

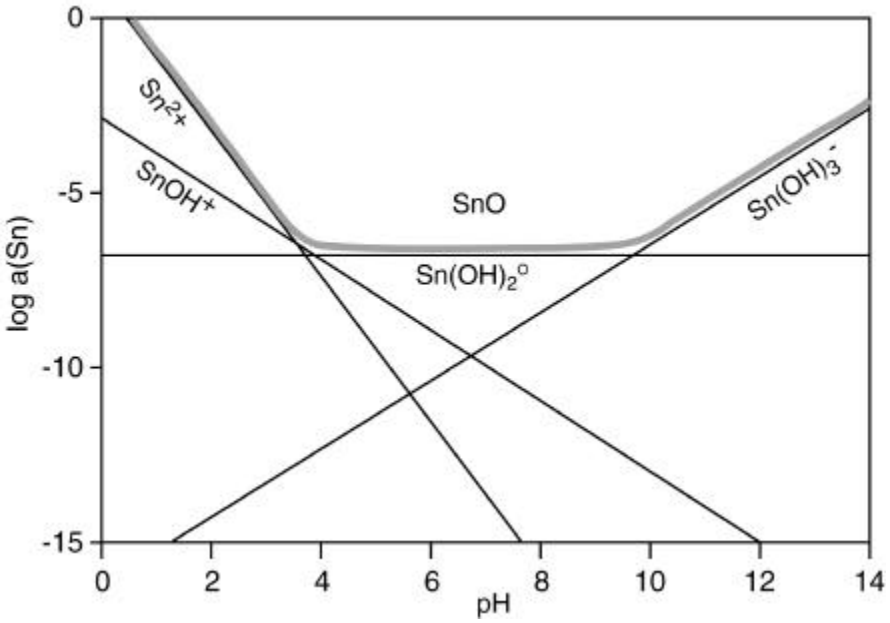

Figure 3.12: Distribution of hydrolysis products in solution saturated with SnO(s) (Séby, et al. 2001).

Romarchite does not appear on this diagram because a solution does not become saturated with respect to SnO(s) until a dissolved tin activity of $10^{-6.73}$ at the pH observed in seawater, 8.2 (**Figure 3.12**). Below this tin activity, SnO(s) dissolves into solution via the following reaction:

$$SnO(s) + H_2O = Sn(OH)_2(aq).$$

Figure 3.13 demonstrates how the $Sn(OH)_2^o$ field shrinks with increased dissolved tin activity as the stability fields of $SnO_2(s)$, stable at higher Eh, and Sn(s), stable at lower Eh, grow at its expense. Thermodynamic calculations adapted from Séby, et al (2001) conclude that the Sn(s) field and the $SnO_2(s)$ field converge at an activity of $10^{-6.59}$. Based on this data, romarchite is only stable over a tin activity range of $10^{-6.73}$ to $10^{-6.59}$. Although dissolved tin activity is rarely this high in the natural environment, the presence of romarchite suggests that within the pore spaces adjacent to a nearly pure tin artifact, these activities could be obtained. Because the stability range of romarchite is quite narrow and falls outside of the stability field of water, it is likely the romarchite has formed metastably. If this is true, romarchite is a metastable step in the oxidation of metallic tin to the formation of cassiterite and exists only due to the sluggish kinetics of the alteration process. Because romarchite has never been observed in the natural environment other than on corroded pure tin materials, it is possible that pure tin is required for its formation. The near absence of native tin in the natural environment suggests that human intervention may be necessary for romarchite formation. The

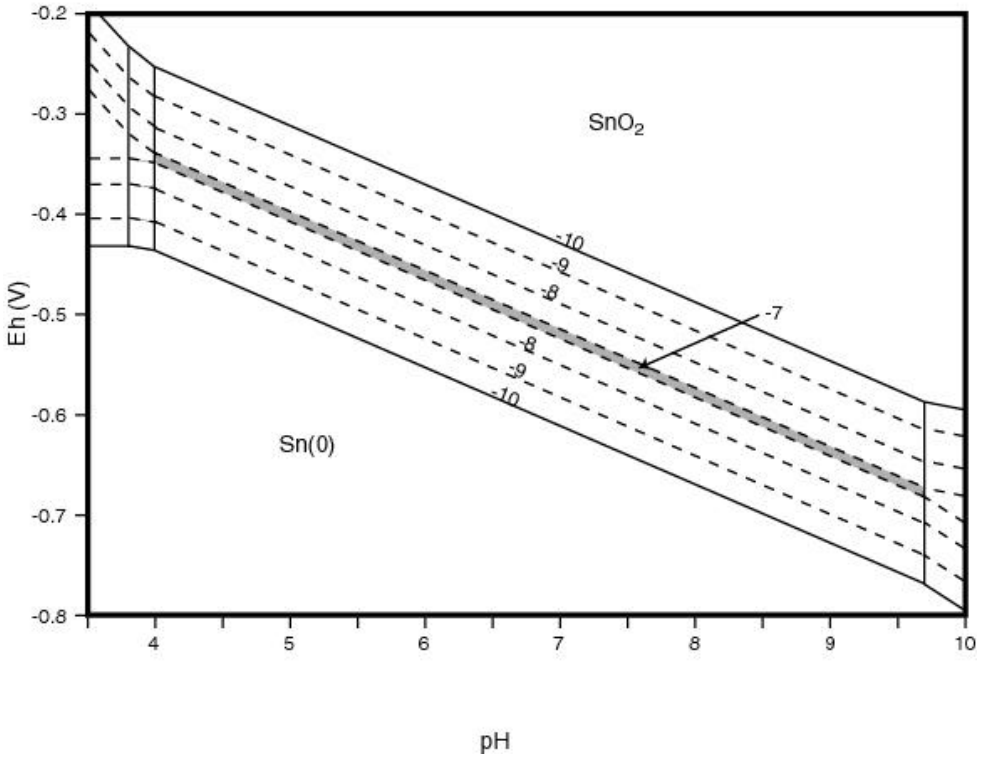

Figure 3.13: Expanded view of $Sn(OH)_2^o$ field (see Figure 3.11). The contours represent the log of the dissolved tin activity. The shaded region represents the stability field of $Sn(OH)_2^o$ at a dissolved tin activity of 10^{-7}.

presence of romarchite on samples corroded in fresh water (Organ and Mandarino 1971), in soils (Williams et al 1998) and in seawater (Dunkle et al, 2002 and this study) suggests that romarchite is a common, yet largely unrecognized, corrosion product of tin in a wide variety of environments. Further information relating to the stability of this mineral and the kinetic properties of its recrystallization into cassiterite will provide valuable information to both archaeologists looking to restore pewter artifacts as well as have industrial applications concerning the passivation of corroding tin.

Conclusion

The study of metallic archaeological artifacts corroding in the natural environment provides an opportunity to observe the long-term processes of metal corrosion that cannot be studied directly in short laboratory time scales. Pewter artifacts from historically dated sites are especially useful in the study of tin corrosion because they provide long-term experiments that extend for times far beyond any that could be carried out in the laboratory, in this case, hundreds of years. All pewter samples appear to undergo corrosion to form surface layers that have commonly been referred as

"pustules" (North 1987). Detailed examination of the corrosion products on pewter artifacts from six different archaeological sites reveals a consistent sequence of tin oxide minerals suggesting that they are the normal alteration products to form on oxidizing pewter. The corrosion process in seawater apparently proceeds by forming abhurite, which slowly alters to romarchite and hydroromarchite. The presence of romarchite and hydroromarchite, without abhurite, on pewter corroded in a fresh water environment (Organ and Mandarino 1971) indicates, however, that abhurite does not have to serve as a precursor to the formation of romarchite and hydroromarchite. The presence of cassiterite on only the most corroded of the artifacts suggests that it may be the ultimate stable phase to form during the corrosion process. This idea is also supported by thermodynamic considerations presented by Séby, et al. (2001). The absence of cassiterite on many of the artifacts is most likely due to the sluggish rate of its formation. If the artifacts had been left in their burial sites and were allowed to reach equilibrium with their surrounding environments, then cassiterite might well have been the only phase observed when corrosion was complete. There are no constraints on the amount of time that it would take for this process to occur but we know from this study that it takes significantly longer than 270-450 years. Although romarchite is not thermodynamically stable under the conditions of burial in seawater, and appears to be metastable under all conditions, because it is observed on nearly all corroding tin artifacts, it may be a required step in the process of the oxidation of tin metal to the final most stable phase of cassiterite. No data is available in the literature for a determination of the stability or metastability of abhurite and hydroromarchite, however, the order of formation of tin corrosion products suggested by textural analysis of all of the phases and thermodynamic analysis of romarchite and cassiterite suggests that these phases, too, will prove to be metastable. Perhaps the study of pewter artifacts from much older archaeological sites could provide insight into the kinetic properties of tin corrosion and improve our understanding of the passivation of metal corrosion in the natural environment.

REFERENCES

Chung, Y.S., Hubenko, A., Meyering, L., Schade, M., Zimmer, J., and Remmel, T. (1997) Morphology and phase of tin oxide thin films during their growth from metallic tin. Journal of Vacuum Science Technology A, 15 (3), May/Jun 1997: 1108-1112.

Craig, J.R. (2001) Ore mineral textures and the tales they tell. Canadian Mineralogist, 39: 937-956.

Craig, J.R., Callahan, J.E., Miller, J.W., and Lusardi, W.R. (2000) Preliminary Studies of some base and precious metals from the *Queen Anne's Revenge*. Southeastern Geology, 40 (7): 41-48.

Craig, J.R. and Vaughan, D.J. (1994) Ore Microscopy and Ore Mineralogy. John Wiley and Sons, NY: 434.

Hatcher, J. and Barker, T.C. (1974) A History of British Pewter. Longman Group Ltd., London.

Lawrence, R.S. and Wilde-Ramsing, M. (2001). In search of Blackbeard: historical and archaeological research at shipwreck site 0003BUI. Southeastern Geology, 40, 1-10.

Lusardi, W.R. (1999) Do the artifacts identify the Beaufort Inlet shipwreck as the pirate Blackbeard's flagship *Queen Anne's Revenge*? Underwater Archaeology, 1999: 123-132.

Lusardi, W.R. (2000) The Beaufort Inlet shipwreck project. The International Journal of Nautical Archaeology, 29 (1): 57-68.

Lusardi, W.R. (forthcoming). Poor Pirate's Silver: Pewterware recovered from Blackbeard's flagship *Queen Anne's Revenge* (1718). The Journal of the Pewter Society. London, forthcoming.

Matzko, J.J., Evans, H.T., Mrose, M.E., and Aruscavage, P. (1985). Abhurite, a new tin hydroxychloride mineral, and a comparative study with a synthetic basic tin chloride. Canadian Mineralogist, 23: 233-240.

North, N.A. (1987) Conservation of metals. Pearson, C., (ed). Conservation of marine archaeological objects. Butterworths, London.

North, N.A. and MacLeod, I.D. (1987) Corrosion of metals. Pearson, C., (ed). Conservation of marine archaeological objects. Butterworths: London.

Organ, R.M. and Mandarino, J. (1971) Romarchite and hydroromarchite, two new stannous minerals. Canadian Mineralogist, 10: 916 (same information published in American Mineralogist, 57: 1555-1556).

Séby, F., Potin-Gautier, M., Giffault, E., and Donard, O.F.X. (2001) A critical review of

thermodynamic data for inorganic tin species. Geochimica et Cosmochimica Acta, 65 (18): 3041-3053.

Williams, W., Sarin, P., Wang, C. and Wisseman, S. (1998) Interpretation of black surface of ancient Chinese bronze mirrors. Abstracts of Presentations at the 31st International Symposium on Archaeometry, Budapest, Hungary.

APPENDIX A

Microprobe Data of Pewter Artifacts and Corrosion Products

Queen Anne's Revenge (1718)

Sample #	Ca	Cl	Sn	Pb	As	Cu	Fe	O	Total
SW44a_00	0.0000	16.8112	70.8199	0.0210	0.0344	0.0478	0.0000	15.3249*	103.0592
SW44a_01	0.0000	15.7821	73.5271	0.0000	0.0277	0.0442	0.0243	6.3775	95.7829
SW44a_02	0.0000	16.0282	71.6949	0.0000	0.0404	0.0341	0.0000	6.0695	93.8671
SW44a_03	0.0000	11.2166	75.6555	0.0360	0.0107	0.0000	0.0448	7.6867	94.6503
SW44a_04	0.0000	0.4349	86.6600	0.0052	0.0000	0.0000	0.0261	11.5919	98.7181
SW44a_05	0.0000	0.0363	88.7236	0.1036	0.0000	0.0000	0.0000	11.9601	100.8236
SW44a_06	0.0000	0.3874	84.9509	0.0000	0.0000	0.1693	0.0464	11.4203	96.9743
SW44a_07	0.0000	0.2218	86.7106	0.0673	0.0000	0.0680	0.0000	11.6612	98.7289
SW44a_08	0.0000	10.1547	76.7327	0.0206	0.0000	0.0827	0.0230	8.0815	95.0952
SW44a_09	0.0000	14.9958	70.3138	0.0770	0.0000	0.0000	0.0150	6.1051	91.5067
SW44a_10	0.0000	0.2669	80.4291	0.0570	0.0191	0.4151	0.0430	10.9093	92.1395
SW44a_11	0.0000	0.3467	80.0744	0.0104	0.0360	2.2502	0.0000	11.2951	94.0128
SW44a_12	0.0000	14.1476	72.9782	0.0926	0.0460	0.1019	0.0335	6.7025	94.1023
SW44a_13	0.0000	0.4312	88.5423	0.0000	0.0238	0.0282	0.0000	11.8533	100.8788
SW44a_14	0.0000	0.0064	83.9062	0.0000	0.0607	0.0105	20.3592	17.1644	121.5074
SW44a_15	0.0000	0.2299	68.2166	0.0000	0.0490	2.4308	0.1941	9.8274	80.9478
SW44a_16	0.0000	0.5200	84.8778	0.0000	0.0000	0.0780	0.0306	11.3530	96.8594
SW44a_17	0.0000	0.3934	86.4769	0.0000	0.0000	0.0000	0.0181	11.5739	98.4623
SW44a_18	0.0000	10.2579	75.6977	0.0515	0.0153	0.0337	0.0000	7.9071	93.9632
SW44a_19	0.0000	0.0740	89.0106	0.0000	0.0198	0.0531	0.0000	12.0020	101.1595
SW44a_20	0.0000	0.0415	89.6817	0.0466	0.0000	0.1194	0.0000	12.1138	102.0030
SW44a_21	0.0000	0.0412	84.3935	0.0696	0.0484	0.0384	20.4195	17.2480	122.2586
SW44a_22	0.0000	10.0266	75.5063	0.0979	0.0000	0.1147	0.0390	7.9637	93.7482
SW44a_23	0.0000	0.2953	77.5171	0.1000	0.0000	1.7577	5.7869	12.4912	97.9482
SW44a_24	0.0000	0.0416	65.7667	0.2334	0.2495	0.1078	0.0000	8.9813	75.3803
SW44a_25	0.0000	0.2597	85.5803	0.1295	0.0943	0.0962	0.0000	11.5424	97.7024
SW44a_26	0.0000	0.2651	82.2839	0.0000	0.0000	0.5382	0.0487	11.1819	94.3178
SW44a_27	0.0000	9.7870	71.4866	0.0103	0.0000	0.0000	0.0000	7.4291	88.7130
SW44a_30		0.2916	80.3104	0.1396	0.0364	0.5231	0.0000	10.9146	92.2157
SW44a_31		0.0359	65.9254	0.1503	0.7356	0.0281	0.0192	9.1387	76.0332
SW44a_32		0.2219	85.6052	0.0361	0.0000	0.0910	0.0000	11.5156	97.4698
SW44a_33		0.3144	85.4434	0.1498	0.0103	0.2201	0.0508	11.5321	97.7209
SW44a_34		0.0816	74.0692	0.0000	0.0000	1.2086	0.0034	10.2717	85.6345
SW44a_35		0.3563	82.5790	0.0000	0.0000	0.0000	0.0000	11.0516	93.9869
SW44a_36		17.3608	73.8702	0.0000	0.0409	0.0698	0.0728	6.0921	97.5066
SW44a_37		12.4680	64.5369	0.0000	0.2556	9.6286	0.0843	8.4168	95.3902
SW44a_38		0.3722	76.2319	0.0000	0.0000	0.0629	0.0463	10.2215	86.9348
SW44a_39		0.1595	88.2826	0.0000	0.0000	0.1571	0.0000	11.9045	100.5037
SW44a_40		*0.1595*	*88.2826*	*0.0000*	*0.0000*	*0.1571*	*0.0000*	*11.9045*	100.5037
SW44a_41		*0.0664*	*89.2434*	*0.0361*	*0.0016*	*0.0116*	*0.0248*	*12.0287*	101.4126
SW44a_42		*17.0648*	*72.6448*	*0.0000*	*0.0000*	*0.0000*	*0.0000*	*5.9422*	95.6518
SW44a_43		*0.1874*	*65.9591*	*0.0570*	*0.6379*	*0.2004*	*0.0000*	*9.1085*	76.1503
SW44a_44		*15.5579*	*73.4631*	*0.0051*	*0.0000*	*0.0797*	*0.0000*	*6.4130*	95.5188
SW44a_45		*7.0441*	*69.8649*	*0.0623*	*0.0274*	*3.0510*	*0.0857*	*8.6349*	88.7703
SW44a_46		*0.0122*	*83.5170*	*0.0053*	*0.0131*	*0.1947*	*19.8297*	*16.9905*	120.5625

Sample #	Ca	Cl	Sn	Pb	As	Cu	Fe	O	Total
SW44a_47		0.0165	84.1342	0.0640	0.0000	0.0521	19.7872	17.0250	121.0790
SW44a_48		0.0184	4.6944	0.0000	53.5577	0.0715	42.7893	30.0620	131.1933
SW44a_49		0.0361	69.0499	0.1040	0.3020	0.2736	2.1997	10.1040	82.0693
SW44a_50		0.0000	95.0880	0.0467	0.0000	2.0929	0.0000	13.3488	110.5764
SW44a_51		0.1232	86.7050	0.0000	0.0000	0.0645	0.0000	11.6767	98.5694
SW44a_52		0.3398	65.7693	0.0000	0.3008	1.0590	0.0441	9.1649	76.6779
SW44a_53		0.6829	85.3709	0.0000	0.0024	0.5951	0.0181	11.5100	98.1794
SW44a_54		1.8972	80.0392	0.0000	0.0196	0.0000	0.0475	10.3815	92.3850
SW44a_55		0.0240	87.2162	0.0000	0.0087	0.1059	0.0056	11.7828	99.1432
SW44a_56		0.8323	87.5767	0.0929	0.0079	0.0066	0.0452	11.6423	100.2039
SW44a_57		13.2793	75.2622	0.0257	0.0234	0.0913	0.0391	7.1929	95.9139
SW44a_58		0.4375	88.2349	0.0000	0.0016	0.2500	0.0373	11.8699	100.8312
SW44a_59		17.0055	75.3534	0.0000	0.0000	0.0000	0.0589	6.3376	98.7554
SW44a_60		14.4389	72.5123	0.1537	0.0203	0.0339	0.0000	6.5437	93.7028
SW44a_61		0.5357	57.4056	0.0000	0.0087	0.1706	0.0000	7.6634	65.7840
SW44a_62		23.4460	72.7579	0.0000	0.0620	0.0824	0.0081	4.5605	100.9169
SW44a_63		0.1087	85.8151	0.0052	0.0000	1.1472	0.0000	11.8330	98.9092
SW44a_64		0.0855	89.3340	0.1859	0.0000	0.0314	0.0418	12.0576	101.7362
SW44a_65		10.0850	72.4539	0.0000	0.0000	0.0775	0.0057	7.5126	90.1347
SW44a_66		23.6885	71.4215	0.0357	0.0000	0.0034	0.0221	4.2926	99.4638
SW44b_01		0.3005	74.5296	0.0000	0.0000	3.5819	0.0578	10.8975	89.3673
SW44b_02		0.2931	66.2709	0.0000	0.0156	7.4644	1.0045	11.0397	86.0882
SW44b_03		0.0240	94.7689	0.0000	0.0459	0.0745	0.0339	12.8130	107.7602
SW44b_04		0.4102	82.9882	0.0363	0.0508	1.1332	0.0532	11.4143	96.0862
SW44b_05		0.2336	80.7586	0.1551	0.0894	0.2367	0.0000	10.9341	92.4075
SW44b_06		0.1749	87.7975	0.0000	0.0000	0.1407	0.0847	11.8557	100.0535
SW44b_07		0.0343	98.3544	0.1757	0.0000	0.0000	0.1671	13.3123	112.0438
SW44b_08		0.0288	90.0672	0.0211	0.0162	0.0751	12.0807	15.6217	117.9108
SW44b_09		18.1894	71.0395	0.1688	0.0104	0.0000	0.0463	5.5016	94.9560
SW44b_10		13.3930	74.5826	0.0000	0.0000	0.0507	0.0092	7.0474	95.0829
SW44b_11		12.3328	72.6799	0.0000	0.0166	0.1048	0.0000	7.0464	92.1805
SW44b_101		0.2284	84.4461	0.1833	0.0000	1.6808	0.0000	11.7695	98.3081
SW44b_102		0.0617	89.8826	0.0000	0.0571	0.1498	0.0000	12.1587	102.3099
SW44b_103		16.504	68.2115	0.0643	0.0552	0.4681	0.0000	Jan-00	90.9147
SW44b_104		17.7480	67.3647	0.0000	0.0000	0.1254	0.0335	5.1174	90.3890
SW44b_105		0.7557	88.4439	0.0883	0.0000	0.0212	0.0164	11.7689	101.0944
SW44b_106		0.2154	87.0455	0.0295	0.0000	0.2027	0.0105	11.7419	99.2455
SW45_01	0.0000	0.0034	83.8206	0.0000	0.0509	0.1064	20.2678	17.1484	121.3975
SW45_02	0.0000	0.0090	99.6506	0.1917	0.0087	0.1244	0.0396	13.4916	113.5156
SW45_03	0.0000	0.0561	96.9453	0.0000	0.0008	0.2259	3.1360	14.0116	114.3757
SW45_04	0.0000	0.1746	90.5593	0.0052	0.0000	0.0299	0.1348	12.2149	103.1187

Sample #	Ca	Cl	Sn	Pb	As	Cu	Fe	O	Total
SW67_01		0.0693	97.8773	0.0500	0.1412	0.0000	0.0208	13.2337	111.3923
SW67_02		0.1093	97.9123	0.0000	0.0484	0.0000	0.0000	13.1898	111.2598
SW67_03		0.0858	65.4119	0.3968	0.6658	0.1502	0.0000	9.0802	75.7907
SW67_04		0.4840	70.8050	0.2766	0.2675	21.4267	0.0677	14.9570	108.2845
SW67_05		0.0923	98.3232	0.1497	0.0000	0.1231	0.0000	13.2761	111.9644
SW67_06		0.1843	36.4529	2.0389	0.0000	0.6666	2.7757	5.9929	48.1113
SW67_07		11.4741	73.7391	0.0225	0.0449	0.0120	0.0000	7.3704	92.6630
SW67_08		11.5174	72.7431	0.1175	0.0099	0.0757	0.0188	7.2439	91.7263
SW67_09		15.5957	64.6657	0.0006	0.3051	0.0486	0.0024	5.3088	85.9269
SW67_10		14.4839	76.7019	0.0952	0.0467	0.0795	0.0248	6.8513	98.2833
SW67_11		12.5062	83.0602	0.0000	0.0168	0.2047	0.0000	8.4318	104.2197
SW67_12		15.9102	69.6388	0.0000	0.0568	0.0798	0.0485	5.8496	91.5837
SW67_13		0.2529	86.3158	0.1220	0.0000	0.0658	0.0231	11.6113	98.3909
SW67_14		0.3094	87.2060	0.0500	0.0071	0.0405	0.0000	11.7023	99.3153
SW67_15		0.2432	86.0603	0.1557	0.0000	0.0000	0.0335	11.5681	98.0608
SW67_16		0.0262	65.5035	0.3014	0.8556	0.0000	0.0000	9.1216	75.8083
SW67_17		0.0067	65.0603	0.3293	0.7704	0.0996	0.0000	9.0662	75.3325
SW67_18		13.2233	75.2205	0.0002	0.0792	1.2770	0.0024	7.5038	97.3064
SW67_19		14.4370	72.1189	0.0000	0.0534	0.1556	0.0000	6.5205	93.2854
SW67_20		0.1116	54.6838	0.0000	0.0000	0.0123	9.0797	9.9508	73.8382
SW67_21		0.2655	84.8069	0.0456	0.0230	0.0000	0.2371	11.4512	96.8293
SW67_22		0.3082	78.7644	0.0631	0.0000	0.1724	0.2985	10.6820	90.2886
SW67_23		0.5807	85.4465	0.0000	0.0000	0.1047	0.0000	11.4139	97.5458
SW67_24		13.8994	74.6701	0.0030	0.0113	0.0656	0.0459	6.9630	95.6583
SW67_25		0.4302	86.1083	0.1545	0.0000	0.1097	0.0150	11.5546	98.3723
SW67_26		0.2703	77.5938	0.3479	0.4977	0.0236	0.0324	10.6005	89.3662
SW67_27		0.3860	86.1633	0.0116	0.0000	0.0726	0.0000	11.5473	98.1808
SW67_28		9.7122	75.0589	0.0000	0.0000	0.0000	0.0000	7.9267	92.6978
SW67_29		12.0413	74.2256	0.0000	0.0577	0.0723	0.0470	7.3390	93.7829
SW67_30		8.3473	78.3104	0.0000	0.0000	0.0239	0.0000	8.6791	95.3607

Sample #		Cl	Pb	Sn	As	Cu	Fe	O	Total
SW11_	1	0.0114	0.0000	98.8836	0.0222	0.0581	0.0000	13.3491	112.3244
SW11_	2	0.0000	0.2884	85.6051	0.2095	0.0598	0.0070	11.6464	97.8162
SW11_	3	0.0109	0.0824	98.7818	0.0000	0.1319	0.0000	13.3533	112.3603
SW11_	4	0.0000	0.0000	98.9436	0.0000	0.0457	0.0128	13.3532	112.3553
SW11_	5	0.0000	0.0000	89.3566	0.0277	0.0862	0.0000	12.0763	101.5468
SW11_	6	0.0288	0.2000	87.5869	0.0174	0.0844	0.0105	11.8459	99.7739
SW11_	7	15.6400	0.0000	70.5072	0.1060	0.0018	0.0000	6.0099	92.2649
SW11_	8	13.2861	0.0000	75.0801	0.0453	0.0324	0.0000	7.1458	95.5897
SW11_	9	14.6619	0.0117	73.8907	0.0045	0.0541	0.0000	6.6683	95.2912
SW11_	10	0.2668	0.1177	86.3181	0.0324	0.0211	0.0000	11.6006	98.3567
SW11_	11	0.0531	0.0059	98.3480	0.0000	0.1285	0.0000	13.2786	111.8141
SW11_	12	0.0298	0.0000	98.6968	0.0269	0.0000	0.0000	13.3067	112.0602
SW11_	13	13.5237	0.0117	75.1607	0.0181	0.2539	0.0000	7.1510	96.1191
SW11_	14	14.6001	0.1051	68.7346	0.0824	0.1337	0.0215	6.0456	89.7230
SW11_	15	13.0374	0.1754	74.5279	0.0030	0.0917	0.0000	7.1424	94.9778
SW11_	16	12.6265	0.0000	74.8969	0.0000	0.0000	0.0166	7.2520	94.7920
SW11_	17	14.0371	0.0000	73.9135	0.0181	0.0757	0.0000	6.8213	94.8657
SW11_	18	0.2055	0.0766	87.0267	0.0000	0.5640	0.0000	11.8331	99.7059
SW11_	19	0.1803	0.0000	89.3889	0.0000	0.0141	0.0105	12.0159	101.6097
SW11_	20	0.1785	0.0118	84.7488	0.0883	1.2180	0.0292	11.7285	98.0031
SW11_	21	0.3867	0.0177	88.5231	0.0166	0.0634	0.0093	11.8714	100.8882
SW11_	22	0.2073	0.0942	87.4720	0.0261	0.0916	0.0000	11.7835	99.6747
SW11_	23	0.2274	0.2354	80.8024	0.0000	0.0158	0.0758	10.8851	92.2419
SW11_	24	0.0340	0.0000	64.8185	0.0000	0.7399	1.4946	9.3446	76.4316
SW11_	25	0.4559	0.2002	85.0840	0.0253	0.1674	0.0222	11.4389	97.3939
SW11_	26	0.0647	0.1531	88.5452	0.0000	0.1497	0.0000	11.9712	100.8839
SW11_	27	0.0062	0.1459	1.4093	56.1009	0.0362	45.9479	31.3439	134.9903
SW11_	28	0.0139	0.0706	98.7168	0.0135	0.0000	0.0222	13.3205	112.1575
SW11_	29	15.8266	0.0000	75.5519	0.0098	0.0976	0.0072	6.6432	98.1363
SW11_	30	12.1708	0.0000	74.3687	0.0000	0.0000	0.0024	7.2796	93.8215
SW11_	31	0.0134	0.0000	83.2293	0.0115	0.2408	20.0366	17.0214	120.5530
SW11_	32	0.0850	0.0000	88.6108	0.0658	0.0211	0.0047	11.9537	100.7411
SW11_	33	0.0363	0.0766	81.4485	0.2526	0.0863	0.0117	11.0833	92.9953
SW11_	34	15.9294	0.0000	72.7663	0.0000	0.0090	0.0000	6.2170	94.9217
SW11_	35	13.2114	0.0760	74.4550	0.0000	0.0288	0.0000	7.0688	94.8400
SW11_	36	17.8316	0.0700	71.6451	0.0758	0.0925	0.0000	5.6874	95.4024
SW11_	37	0.0164	0.1356	97.4138	0.1015	0.0388	0.6332	13.3623	111.7016
SW11_	38	0.0123	0.0789	85.6048	5.8420	0.1531	5.9251	15.1507	112.7669
SW11_	101	0.0042	0.0370	95.1665	0.0603	0.8152	0.0000	13.0553	109.1385
SW11_	102	0.0000	0.1448	95.8632	0.0137	1.4831	0.0417	13.3237	110.8702
SW11_	103	0.0184	0.0000	89.5715	2.9110	2.0981	2.0037	14.1053	110.7080
SW11_	104	0.0093	0.1211	97.9290	0.0000	0.2337	0.0227	13.2739	111.5897
SW11_	105	0.0000	0.0000	92.0251	0.0237	1.6701	4.6090	14.1540	112.4819

St. Johns Bahamas (~1550)

Sample #	Sn	Cl	As	Cu	Fe	Pb	O	Total
SW52_01	98.5399	0.0392	0.0000	0.2801	0.0185	0.1721	13.3639	112.4137
SW52_02	99.2464	0.0448	0.0000	0.1163	0.0000	0.1814	13.4120	113.0009
SW52_03	98.9480	0.0917	0.0000	0.0000	0.0000	0.1472	13.3293	112.5162
SW52_04	82.1531	0.0393	0.0000	0.0000	19.4544	0.3091	16.6632	118.6191
SW52_05	0.4646	0.0000	0.0000	0.0114	0.0371	68.5645	5.3707	74.4483
SW52_06	76.8422	9.4984	0.0000	0.0411	0.0070	0.0431	8.2310	94.6628
SW52_07	75.1207	9.1569	0.0000	0.0257	0.0000	0.1066	8.0750	92.4849
SW52_08	78.4210	11.8801	0.0000	0.0000	0.0000	0.0000	7.8908	98.1919
SW52_09	77.0006	9.6180	0.0000	0.0000	0.0000	0.0000	8.2097	94.8283
SW52_10	85.4369	0.4131	0.0000	0.0000	0.0323	0.5527	11.4760	97.9110
SW52_11	86.4141	0.2929	0.0273	0.0084	0.0069	0.4670	11.6318	98.8484
SW52_12	85.7052	0.3265	0.0000	0.0000	0.0000	0.7030	11.5341	98.2688
SW52_13	77.2398	0.1609	0.0000	0.1126	0.0346	1.7256	10.5475	89.8210
SW52_14	81.9261	0.2120	0.0000	0.0740	0.0173	2.0445	11.1776	95.4515
SW52_15a	81.9206	0.1662	0.0058	0.2949	0.0000	0.7783	11.1420	94.3078
SW52_15b	82.7772	0.2259	0.0000	0.0000	0.0127	0.7460	11.1690	94.9308
SW52_16	76.0139	0.3755	0.0000	0.0685	0.0218	5.8707	10.6391	92.9895
SW52_17	85.5935	0.3028	0.0000	0.0034	0.0831	1.0547	11.5762	98.6137
SW52_18	0.1365	0.0000	0.0000	0.0128	0.0000	69.1567	5.3619	74.6679
SW52_19	72.7690	0.4417	0.0000	0.3218	0.1293	6.9925	10.3679	91.0222
SW52_20	83.0057	0.1914	0.0000	0.0707	0.0000	1.1290	11.2513	95.6481
SW52_21	81.7456	0.2279	0.0000	0.0556	0.0000	0.5983	11.0285	93.6559
SW52_22	66.8840	0.2423	0.0000	0.0694	0.6243	11.7825	10.0678	89.6703
SW52_23	61.7397	1.4849	0.0000	0.8141	0.3913	17.1754	9.6311	91.2365
SW52_24	78.7181	0.3634	0.0000	0.0000	0.0000	4.8765	10.9061	94.8641
SW52_25	77.1895	10.2747	0.0000	0.0103	0.0000	0.0000	8.0896	95.5641
SW52_26	1.1668	0.0000	0.0000	0.0000	0.0341	67.3600	5.3686	73.9295
SW52_27	80.2560	2.9824	0.0000	5.8280	0.0151	0.0958	11.6250	100.8023
SW52_28	79.5723	2.9999	0.0000	5.9789	0.0431	0.2371	11.5858	100.4171
SW52_29	80.7180	1.0761	0.0000	0.0473	0.0567	0.0323	10.6690	92.5994
SW52_30	85.6927	0.3674	0.0000	0.0456	0.0000	0.2093	11.4965	97.8115
SW52_31	85.7622	0.1901	0.0000	0.0691	0.0069	0.4854	11.5751	98.0888
SW52_32	79.1957	0.9247	0.0000	0.2705	0.0197	0.0966	10.5485	91.0557
SW52_33	88.6249	0.2471	0.0000	0.0135	0.0497	0.0141	11.9100	100.8593
SW52_34	87.5430	0.2684	0.0000	0.0506	0.0000	0.0959	11.7608	99.7187
SW52_35	86.1648	0.3376	0.0000	0.0793	0.0000	0.0600	11.5638	98.2055
SW52_36	79.1367	1.2116	0.0000	0.1640	0.0093	0.1702	10.4517	91.1435
SW52_37	87.0137	5.9717	0.0000	0.0493	0.0000	0.5633	10.4383	104.0363
SW52_38	83.6088	0.2609	0.0000	0.0000	0.0000	1.2794	11.3108	96.4599
SW52_ 101	91.1694	0.3916	0.0000	0.0000	10.6065	1.1118	15.3262	118.6055
SW52_ 102	85.3382	0.1207	0.0000	0.0000	19.7899	0.5135	17.1861	122.9484
SW52_ 103	86.4780	0.0472	0.0000	0.6302	16.5994	0.3166	16.5857	120.6571
SW52_ 104	86.1332	0.2684	0.0383	0.1986	0.0000	1.1231	11.6996	99.4612

La Capitana (1715)

Sample #	Cl	Sn	Pb	As	Cu	Fe	Ca	S	O	Total
SW25_1	0.5353	75.0006	1.2236		0.7258	0.0000	0.0319	0.0651	20.4550	97.5020
SW25_2	0.7686	71.7727	0.3922		1.7279	0.0512	0.6776	0.0000	19.9277	94.5493
SW25_3	1.0331	71.1602	0.4340		1.7754	0.0000	0.8894	0.1525	19.9402	94.3517
SW25_4	17.8561	63.4230	0.0000		4.0879	0.0062	0.0000	0.0819	14.1829	81.7819
SW25_5	14.6733	74.4228	0.0137		0.1206	0.0234	0.0000	0.0000	16.7921	91.3726
SW25_6	17.0181	67.3493	0.0000		2.4115	0.0000	0.0000	0.0020	14.9271	84.6899
SW25_7	0.8252	72.2936	0.2948		1.2783	0.0183	0.6570	0.0332	19.9500	94.5252
SW25_8	1.2024	72.4371	0.2253		1.0356	0.0000	0.7856	0.0953	19.9452	94.5241
SW25_9	15.4265	66.7468	0.0723		3.0833	0.0000	0.0000	0.0297	15.3261	85.2582
SW25_10	0.4420	83.0209	0.3732		0.0255	0.0243	0.0000	0.0413	22.3669	105.8521
SW25_11	0.0844	0.1463	0.0000		0.0000	0.0000	36.9924	0.3800	15.1670	52.6857
SW25_12	0.0000	0.2922	65.8382		0.1129	0.0000	0.0345	7.3064		73.5842
SW25_13	0.0000	0.1703	68.4739		0.0423	0.0055	0.0067	7.8055	13.1392	89.6434
SW25_14	0.0000	0.1220	68.7865		0.1186	0.0783	0.0308	7.6202	13.0151	89.7715
SW25_15	1.2304	66.3199	4.6606		1.5235	0.0000	0.1807	0.0402	18.4585	91.1834
SW25_16	1.2405	66.8849	4.6522		1.3426	0.0000	0.1850	0.1102	18.6340	91.8089
SW25_17	0.2375	98.4190	0.0784		0.1443	0.0178	0.0000	0.0059		98.6654
SW25_18	0.2852	97.2674	0.0327		0.0000	0.0000	0.0000	0.0205		97.3206
SW57a_01	0.3440	97.4210	0.0000	0.0000	0.2550	0.0200	0.0000		13.1250	110.8210
SW57a_02	0.2690	98.6070	0.0050	0.0080	0.0350	0.0670	0.0000		13.2630	111.9850
SW57a_03	0.2880	98.0980	0.1230	0.0000	0.1810	0.0000	0.0000		13.2140	111.6160
SW57a_04	0.2570	97.5370	0.0200	0.3580	0.0170	0.0130	0.0000		13.2140	111.1590
SW57a_05	10.4660	71.9810	0.0250	0.0000	0.2240	0.0580	0.0000		7.4170	79.7050
SW57a_06	5.0180	76.1240	0.0560	0.0000	0.0250	0.0160	0.0000		9.1450	85.3660
SW57a_07	11.3730	71.5980	0.0000	0.0000	0.0000	0.0000	0.0000		7.0850	78.6830
SW57a_08	0.1160	74.8400	0.0620	0.6030	0.9910	0.0800	0.0000		10.5330	87.1090
SW57a_09	7.0270	72.1860	0.0000	0.0000	0.1090	0.0270	0.0000		8.1800	80.5020
SW57a_10	11.1970	75.1470	0.0710	0.0000	0.0090	0.0220	0.0000		7.6180	82.8670
SW57a_11	0.0770	76.6240	0.1480	0.0000	0.1440	0.0370	0.0000		10.3700	87.3230
SW57a_12	0.1460	75.8840	0.0620	0.0530	0.7300	0.0260	0.0000		10.4090	87.1640
SW57a_13	2.5240	77.7200	0.1690	0.0000	0.0810	0.0220	0.0000		9.9470	87.9390
SW57a_14	13.5870	74.5090	0.0000	0.0000	0.0240	0.0070	0.0000		6.9860	81.5260
SW57a_16	0.0550	76.0860	0.0310	0.0380	0.8010	0.0330	0.0000		10.4700	87.4590
SW57a_17	0.0600	76.0070	0.1430	0.0030	0.6950	0.0020	0.0000		10.4200	87.2700
SW57a_18	0.5070	66.2850	0.3400	12.1260	24.3640	0.0180	0.0000		18.8720	122.0050
SW57a_19	0.5440	98.1160	0.0560	0.0000	0.0000	0.0100	0.0000		13.1110	111.2930
SW57a_20	18.2980	76.2580	0.1010	0.0040	0.0000	0.0240	0.0000		6.1670	82.5540
SW57a_21	0.3340	76.0360	0.1380	0.0000	0.7290	0.0100	0.0000		10.3720	87.2850
SW57a_22	10.6930	75.5630	0.0000	0.0000	0.0740	0.0170	0.0000		7.7970	83.4510
SW57a_23	16.6860	72.0390	0.1320	0.9130	0.0000	0.0140	0.0000		6.2530	79.3510
SW57a_24	0.3130	72.3860	0.6620	0.0000	0.8700	0.0000	0.8280		10.2880	85.0340
SW57a_25	0.3660	74.2560	1.1740	0.2970	0.7130	0.0000	0.2430		10.3890	87.0720
SW57a_26	0.8470	73.8980	0.3840	0.0480	0.2280	0.0000	0.3970		10.0320	84.9870
SW57a_27	0.5730	84.3850	0.3530	0.0000	0.1530	0.0000	0.0000		11.3120	96.2030
SW57a_28	0.5670	83.4200	0.7670	0.0000	0.0240	0.0000	0.0000		11.1830	95.3940
SW57a_29	0.4330	85.6370	0.5010	0.0000	0.0760	0.0570	0.0000		11.5210	97.7920
SW57a_30	0.0690	75.5020	0.0100	0.5770	1.3090	0.0270	0.0000		10.6850	88.1100
SW57a_31	0.7330	77.9670	0.0000	0.0180	0.2510	0.0500	0.0000		10.4280	88.7140

Sample #	Cl	Sn	Pb	As	Cu	Fe	Ca	S	O	Total
SW57a_32	18.0900	68.5520	0.1270	0.0000	0.6350	0.0000	0.0000		5.3290	74.6430
SW57a_33	13.5700	73.7020	0.0000	0.0900	0.6700	0.0400	0.0000		7.0820	81.5840
SW57a_34	0.1060	72.6910	0.3390	0.1900	1.1320	0.0160	0.0000		10.1520	84.5200
SW57a_35	0.2640	87.9590	0.1070	0.0000	0.0660	0.0210	0.0000		11.8280	99.9810
SW57a_36	0.298	84.5970	0.3990	0.0110	0.0740	0.0350	0.0000		11.4000	96.5160
SW57a_37	0.3910	86.6400	0.1890	0.0270	0.0370	0.0220	0.0000		11.6300	98.5450
SW57a_38	0.3510	77.5410	1.1820	0.0000	0.4690	0.0000	0.0000		10.5830	89.7750
SW57a_39	0.2410	77.3890	1.6400	0.0000	0.0250	0.0190	0.0000		10.5160	89.5890
SW57a_40	0.4060	82.0380	0.9760	0.0000	0.0000	0.0000	0.0000		11.0430	94.0570
SW57b_01	0.0380	0.2000	98.0140	0.0000	0.0300	0.0060	0.0320		7.6090	105.8910
SW57b_02	0.0000	0.1050	0.2900	0.0330	0.2610	96.4900	0.0210		27.7650	124.9650
SW57b_03	13.7440	0.2490	77.5120	0.0110	0.0030	0.0000	0.0000		2.9220	80.6970
SW57b_04	0.3460	0.0440	79.9570	0.0000	0.0210	0.0000	0.0540		6.1290	86.2050
SW57b_05	0.0700	0.0540	78.3950	0.0130	0.0000	0.0000	0.0100		6.0530	84.5250
SW57b_06	0.3420	0.1300	82.4560	0.0000	2.2450	0.0040	0.0630		6.8990	91.7970
SW57b_07	0.5630	0.1020	95.0290	0.0000	0.0380	0.0080	0.0720		7.2650	102.5140
SW57b_08	0.0420	0.0000	29.7670	0.1630	0.3010	0.0000	37.9380		17.5620	85.7310
SW57b_09	14.5040	0.1260	78.1150	0.0010	0.0190	0.0000	0.0080		2.7840	81.0530
SW57b_10	0.0410	0.2310	98.9470	0.0000	0.0830	0.0020	0.0000		7.6840	106.9470
SW57b_11	0.2110	0.2630	95.2850	0.0120	0.0000	0.0640	0.0170		7.3750	103.0160
SW57b_12	7.2410	1.8880	79.6330	0.0000	0.0200	0.0350	0.0000		4.7850	86.3610
SW25_ 101	16.1083	72.2983	0.0000	0.0378	0.8406	0.0000			6.3351	95.6201
SW25_ 102	0.3591	87.1457	0.0769	0.0000	0.1271	0.0000			11.7046	99.4134
SW25_ 103	0.8367	81.9677	0.4307	0.0000	0.2731	0.3786			11.0713	94.9581
SW25_ 104	0.8010	72.7023	0.1234	0.1447	0.8661	0.0000			9.8938	84.5313
SW25_ 105	0.8265	73.7389	0.1903	0.0016	1.2503	0.0176			10.0889	86.1141
SW25_ 106	0.4147	76.9186	0.7756	0.0168	0.9308	0.0050			10.5765	89.6380
SW25_ 107	0.4234	77.1208	2.2814	0.0000	0.1142	0.0000			10.5056	90.4454
SW25_ 108	0.0665	0.1131	0.0000	0.0000	0.1371	0.0000			0.0348	0.3515
SW25_ 109	0.5035	80.5679	0.4311	0.0184	0.4846	0.0591			10.9254	92.9900
SW25_ 110	1.0817	72.4302	0.2573	0.1160	1.1488	0.0000			9.8661	84.9001
SW25_ 111	17.3326	71.7999	0.0152	0.0000	0.0184	0.0090			5.7762	94.9513
SW25_ 112	1.2061	71.5311	0.3242	0.3214	0.8828	0.0454			9.7338	84.0448
SW25_ 113	1.2171	69.5849	0.1287	0.0769	1.3340	0.0000			9.4762	81.8178
SW25_ 114	0.8610	72.6029	0.1805	0.0097	1.9034	0.0000			10.0892	85.6467
SW25_ 115	0.5770	82.4772	0.3746	0.0271	0.3979	0.0000			11.1259	94.9797
SW25_ 116	0.3234	86.1520	0.1796	0.0000	0.1555	0.0038			11.5948	98.4091
SW25_ 117	0.3830	99.4720	0.0000	0.0096	0.0535	0.0000			13.3394	113.2575
SW25_ 118	1.6324	98.6176	0.0000	0.0000	0.0077	0.0252			12.9349	113.2178

San Jose (1733)

Sample #	Sn	Ca	Cl	As	Cu	Fe	Pb	S	O	Total
SW26_1	77.6077	0.0956	0.0247		0.0366	0.4647	0.0519	0.1272	21.2296	99.6380
SW26_2	77.1586	0.1900	0.0119		0.0274	0.5999	0.0000	0.0683	21.1200	99.1761
SW26_3	77.6216	0.1216	0.0207		0.0914	0.4416	0.0000	0.0734	21.1914	99.5617
SW26_4	77.4045	0.0845	0.0158		0.0000	0.0438	0.0000	0.1405	21.0519	98.7410
SW26_5	77.8559	0.0000	0.0948		0.0000	0.0231	0.0000	0.1560	21.1316	99.2614
SW26_6	0.1636	0.6118	0.0149		0.0000	61.6327	0.0428	1.2236	19.1671	82.8565
SW26_7	0.1101	0.6062	0.0538		0.0000	61.6011	0.0311	1.2144	19.1226	82.7393
SW26_8	0.1813	0.6297	0.0480		0.0217	62.1804	0.0000	1.0991	19.2064	83.3666
SW26_9	0.0871	41.3997	0.0000		0.0604	1.4361	0.0000	0.6907	17.6663	61.3403
SW26_10	0.0654	42.6446	0.0000		0.0604	1.4542	0.0000	0.6951	19.1670	64.0867
SW26_11	0.0762	40.6161	0.0141		0.0000	5.1703	0.0000	0.9063	18.6172	65.4002
SW26_12	0.0156	40.2273	0.0076		0.0395	2.6329	0.0000	0.8157	17.6396	61.3782
SW26_13	0.0000	0.7315	0.0331		0.0543	61.9590	0.0000	0.9377	18.9851	82.7007
SW26_14	0.0544	35.9479	0.0053		0.0000	0.5334	0.0000	0.3248	14.8409	51.7067
SW26_15	0.0016	37.6016	0.0000		0.0489	0.4046	0.0000	0.2833	15.4220	53.7620
SW26_16	0.1304	35.3056	0.0288		0.0000	1.1297	0.0000	0.1811	14.6271	51.4027
SW26_17	0.0513	38.3336	0.0277		0.0000	0.2322	0.0664	0.1992	15.5808	54.4912
SW26_18	0.3410	18.8404	0.0000		0.0658	28.8713	0.0000	8.5149	24.4000	81.0334
SW31_ 101	95.5180		0.0173	0.1329	3.2179	0.0416	0.0414		13.7402	112.7093
SW31_ 102	98.9482		0.0231	0.2456	0.1939	0.0000	0.0411		13.4641	112.9160
SW31_ 103	98.5592		0.0397	0.0776	0.0280	0.0063	0.0821		13.3173	112.1102
SW31_ 104	98.3812		0.0303	0.0000	0.2219	0.0176	0.2208		13.3333	112.2051
SW31_ 105	71.5779		15.1059	0.3088	0.3141	0.0000	0.0000		6.4184	93.7251
SW31_ 106	68.1285		16.1741	0.2932	3.8195	0.0477	0.0720		6.6092	95.1442
SW31_ 107	74.5797		12.6763	1.0007	0.0600	0.0205	0.0512		7.5387	95.9271
SW31_ 108	74.3267		14.7977	0.4089	0.0366	0.0000	0.2193		6.8376	96.6268
SW31_ 109	72.0043		17.6127	0.2829	0.1208	0.0026	0.0000		5.8540	95.8773
SW31_ 110	73.6702		0.2691	0.2511	0.1196	0.0000	1.5850		10.1033	85.9983
SW31_ 111	73.4380		0.3051	0.2294	0.5221	0.0113	1.5769		10.1609	86.2437
SW31_ 112	77.0566		0.2648	0.0854	0.0841	0.0277	0.4208		10.4168	88.3562
SW31_ 113	89.0574		0.3337	0.0104	0.0638	0.0289	0.0565		11.9621	101.5128
SW31_ 114	87.4886		0.2468	0.0000	0.0561	0.0000	0.2770		11.7737	99.8422
SW31_ 116	87.1203		0.1882	0.0000	0.0459	0.0000	0.4156		11.7454	99.5154
SW31_ 117	87.7798		0.3915	0.0215	0.1427	0.0000	0.7590		11.8462	100.9407
SW31_ 118	59.7239		0.1188	0.0000	2.5849	0.5217	0.7204		8.8802	72.5499
SW31_ 119	0.0803		0.0325	0.0000	0.0000	0.0000	0.0357		0.0062	0.1547
SW31_ 120	83.8805		0.4272	0.0000	0.1632	0.0000	0.2258		11.2696	95.9663
SW31_ 121	84.8162		0.3478	0.0000	0.0280	0.0239	0.3899		11.3991	97.0049
SW31_ 122	88.5957		0.2432	0.0000	0.0000	0.0088	0.3437		11.9173	101.1087
SW31_ 123	83.2507		0.4502	0.0072	0.0077	0.0239	0.2616		11.1523	95.1536
SW31_ 124	80.4070		0.4892	0.0000	0.0612	0.0151	0.3078		10.7723	92.0526
SW31_ 125	87.217		0.5401	0.0175	0.0000	0.0163	0.9124		11.7161	100.4194
SW31_ 126	85.6330		0.4929	0.0279	0.0000	0.0000	0.7179		11.4969	98.3686
SW31_ 127	83.1561		0.3154	0.0000	0.0000	0.0038	0.5486		11.1821	95.2060
SW31_ 128A	86.2879		0.2184	0.0000	0.0000	0.0063	0.4001		11.6154	98.5281
SW31_ 128B	77.8697		0.4095	0.0000	0.1070	0.0138	0.8103		10.4983	89.7086
SW31_ 129	73.6255		0.0094	28.6112	1.8310	0.0115	0.5435		19.5944	124.2265
SW31_ 130	72.3919		0.0178	29.2740	0.5371	0.1413	0.0000		19.3079	121.6700
SW31_ 131	99.4472		0.7824	0.0814	0.2017	0.0000	0.0359		13.3090	113.8576
SW31_ 132	99.1842		0.0203	0.1040	0.0000	0.0302	0.0257		13.4098	112.7742
SW31_ 133	73.9393		16.3294	0.0770	0.0707	0.0283	0.0865		6.3399	96.8711
SW31_ 134	90.4422		0.0610	0.0000	0.0000	0.1849	0.0924		12.2384	103.0189

Port Royal, Jamaica (1692)

Sample #		Cl	Sn	Pb	As	Cu	Fe	O	Total
SW70_	1	0.0106	96.5662	0.3370	2.5475	1.5187	0.0000	14.2396	115.2196
SW70_	2	0.0083	64.2677	0.0734	0.0203	39.1010	0.1194	18.5531	122.1432
SW70_	3	0.0100	100.4277	0.3125	0.1782	0.0739	0.0236	13.6424	114.6683
SW70_	4	0.0000	83.3241	0.0700	0.0290	0.0376	20.7309	17.1959	121.3875
SW70_	5	0.0010	83.9527	0.0700	0.0000	0.1606	20.9321	17.3598	122.4762
SW70_	6	0.0063	97.5233	0.3306	0.0000	3.7087	0.0130	14.1082	115.6901
SW70_	7	0.0010	99.4264	0.2707	0.0080	0.1001	0.0000	13.4516	113.2578
SW70_	8	0.1226	69.1588	0.1979	0.0000	0.0000	0.1631	9.3572	78.9996
SW70_	9	0.0277	94.2830	0.2967	0.0000	0.0000	0.0390	12.7376	107.3840
SW70_	10	0.1054	73.8653	1.5041	0.0000	0.2666	0.1946	10.1726	86.1086
SW70_	11	0.0110	97.8097	0.3435	0.0000	0.0000	0.0201	13.2150	111.3993
SW70_	12	0.0107	4.6451	81.5152	0.0038	0.1080	0.0475	6.9603	93.2906
SW70_	13	0.0000	5.1114	93.7199	0.0000	0.4669	0.0000	8.0436	107.3418
SW70_	14	0.2315	52.2030	13.6184	0.0730	0.1179	0.1047	8.1197	74.4682
SW70_	15	0.0512	67.5050	3.0212	0.0000	0.0548	1.3330	9.7174	81.6826
SW70_	16	0.1077	63.5781	3.0237	0.0000	0.0000	0.9761	9.0595	76.7451
SW70_	17	0.0119	2.7579	0.0515	53.0715	0.0027	44.7244	30.1877	130.8076
SW70_	18	0.1048	81.4134	2.5715	0.0381	0.0522	0.0589	11.1920	95.4309
SW70_	19	0.6332	6.7739	0.1096	0.0000	0.0049	0.2390	0.8484	8.6090
SW70_	20	0.0192	3.5023	0.1791	0.0000	0.0000	0.2377	0.5497	4.4880
SW70_	21	0.0106	4.5300	0.0939	0.0000	0.0000	0.0401	0.6270	5.3016
SW71_	1	14.6125	74.0800	0.0000	0.0000	0.0416	0.0302	6.7081	95.4724
SW71_	2	0.0917	99.7508	0.0991	0.0000	0.0000	0.0095	13.4365	113.3876
SW71_	3	0.1166	98.7657	0.1201	0.0000	0.0813	0.0817	13.3409	112.5063
SW71_	4	0.0616	99.4528	0.0052	0.0000	0.1100	0.0746	13.4422	113.1464
SW71_	5	0.0597	98.5517	0.0261	0.0000	0.0000	0.0391	13.2849	111.9615
SW71_	6	0.0700	74.1228	2.9371	0.0000	0.3496	0.0000	10.2911	87.7706
SW71_	7	0.0747	71.1535	2.9575	0.0360	1.3586	0.0425	10.1691	85.7919
SW71_	8	16.2045	24.6437	44.1481	0.0170	0.0767	0.0090	3.1020	88.2010
SW71_	9	16.2769	69.7276	0.0724	0.0000	0.0000	0.0109	5.7354	91.8232
SW71_	10	16.1552	73.9583	0.1760	0.0000	0.0000	0.0145	6.3422	96.6462
SW71_	11	1.0000	74.7964	0.3246	0.1019	1.1085	0.0000	10.1940	87.5254
SW71_	12	0.5270	75.1974	0.3507	0.0185	0.9538	0.0000	10.2912	87.3386
SW71_	13	17.2136	73.5758	0.0673	0.0174	0.0000	0.0000	6.0448	96.9189
SW71_	14	0.3986	79.8522	2.5612	0.0191	0.0000	0.0035	10.8794	93.7140
SW71_	15	0.3077	84.5400	0.9232	0.0152	0.1382	0.0000	11.4127	97.3370
SW71_	16	0.2567	80.9250	1.4597	0.0311	0.0310	0.0024	10.9821	93.6880
SW71_	17	10.8658	73.1479	0.0000	0.0000	0.0122	0.0313	7.4208	91.4780
SW71_	18	1.2155	75.6870	0.3807	0.0000	0.0024	0.0000	9.9587	87.2443
SW71_	19	10.4954	75.4342	0.0000	0.0000	0.0000	0.0000	7.8006	93.7302
SW71_	20	11.0187	74.3479	0.0260	0.0000	0.0000	0.0000	7.5381	92.9307
SW71_	21	0.2533	3.2899	66.4282	0.0000	0.0041	0.0000	5.5169	75.4924
SW71_	22	0.0000	0.0891	68.1816	0.0006	0.0303	0.0000	8.2848	76.5864
SW71_	23	13.1548	73.0336	0.0052	0.0000	0.0000	0.0000	6.8773	93.0709
SW71_	24	1.3066	75.5892	0.4434	0.0000	0.0000	0.0308	9.9380	87.3080
SW71_	25	0.9507	85.3474	0.6939	0.0000	0.0574	0.0000	11.3587	98.4081
SW71_	26	0.2746	88.1009	0.2662	0.0000	0.0000	0.0118	11.8384	100.4919

Sample #		Cl	Sn	Pb	As	Cu	Fe	O	Total
SW72_	1	0.0883	98.6817	0.0886	0.0432	0.1670	0.0000	13.3456	112.4144
SW72_	2	0.1199	90.6597	0.0372	0.0389	8.8991	0.3671	14.5555	114.6774
SW72_	3	0.0411	1.2552	0.0710	55.1685	0.0437	47.4605	31.4460	135.4860
SW72_	4	13.0999	74.8193	0.1294	0.0145	0.0366	0.0205	7.1597	95.2799
SW72_	5	14.3575	74.8965	0.0000	0.0198	0.0195	0.0000	6.8679	96.1612
SW72_	6	2.0195	75.8629	0.2037	0.5251	0.1535	0.3003	10.0796	89.1446
SW72_	7	1.7445	76.0089	0.0000	0.2774	0.0048	0.1684	9.9910	88.1950
SW72_	8	2.4604	70.4016	0.1048	0.0705	1.9001	0.1094	9.4757	84.5225
SW72_	9	16.2566	74.0054	0.0620	0.0159	0.0000	0.0000	6.3178	96.6577
SW72_	10	9.1696	75.2167	0.0986	0.0271	0.0000	0.0132	8.0905	92.6157
SW72_	11	0.4142	87.8470	0.0782	0.0280	0.0000	0.0248	11.7708	100.1630
SW72_	12	0.9759	85.3533	0.0834	0.0000	0.0000	0.0793	11.3150	97.8069
SW72_	13	1.8597	86.2077	0.0052	0.0000	0.1054	0.0000	11.2285	99.4065
SW72_	14	0.2849	82.5727	0.1199	0.0000	0.0143	0.0142	10.9490	93.9550
SW72_	15	0.2400	88.2597	0.0000	0.0000	0.0669	0.0000	11.8605	100.4271
SW72_	16	0.2562	87.7923	0.0627	0.0080	0.0550	0.0036	11.7993	99.9771
SW72_	17	0.2117	98.9475	0.0000	0.0016	0.0287	0.0284	13.3067	112.5246
SW72_	18	10.4279	75.0578	0.0104	0.0000	0.0097	0.0012	7.7687	93.2757
SW72_	19	0.5192	85.9647	0.2297	0.0296	0.0000	0.0000	11.4985	98.2417
SW72_	20	0.4317	79.2341	0.0835	0.0000	0.0478	0.0071	10.6042	90.4084
SW72_	21	0.3457	83.4857	0.0731	0.0329	0.0000	0.0308	11.2012	95.1694
SW72_	22	0.2854	87.3779	0.1044	0.0104	0.0000	0.0308	11.9348	99.7437
SW72_	23	0.9724	84.8628	0.0783	0.0000	0.0263	0.0000	11.2331	97.1729
SW72_	24	0.3079	87.4822	0.0731	0.0000	0.0646	0.0000	11.7454	99.6732
SW72_	25	9.0262	75.4716	0.0000	0.0101	0.0121	0.0204	8.1493	92.6897
SW72_	26	9.1963	74.9880	0.0000	0.0000	0.1021	0.0000	8.0593	92.3457

Henrietta Marie (1701)

Sample #		Sn	Cl	As	Cu	Fe	Pb	O	Total
SW53_01		83.7314	0.1248	0.0000	0.0169	0.0000	0.0853	11.2700	95.2284
SW53_02		83.4127	0.1705	0.0971	0.1604	0.0625	0.0000	11.2953	95.1985
SW53_03		77.7313	0.2035	0.1416	1.0667	0.2582	0.0689	10.8259	90.2961
SW53_04		78.7265	0.3034	0.1212	6.6185	0.0523	0.0509	12.2684	98.1412
SW53_04a		87.8888	0.0000	0.0000	0.4796	0.0000	0.0768	11.9745	100.4197
SW53_05		87.3021	0.2106	0.0000	0.0101	0.0139	0.0000	11.7277	99.2644
SW53_06		86.1047	0.1997	0.0000	0.0068	0.0000	0.0000	11.5639	97.8751
SW53_07		86.6473	0.4602	0.0000	0.0000	0.0035	0.0470	11.5812	98.7392
SW53_08		87.8365	0.2610	0.0000	0.0000	0.0324	0.0000	11.7911	99.9210
SW53_09		83.2073	0.0018	0.0000	0.0977	20.6024	0.0845	17.1499	121.1436
SW53_10		87.6293	0.1199	0.0100	0.1232	0.0000	0.0347	11.8227	99.7398
SW53_11		88.3528	0.2028	0.0266	0.1942	0.0069	0.0119	11.9249	100.7201
SW53_12		87.9079	0.1865	0.0548	0.3125	0.0127	0.0000	11.9082	100.3826
SW53_13		63.8841	0.0142	0.0000	36.3520	0.6799	0.0467	17.9600	118.9369
SW53_14		63.9910	0.0117	0.0200	37.3489	0.5909	0.0400	18.2063	120.2088
SW53_15		82.8701	0.1109	0.0000	8.6052	0.0000	0.0886	13.3197	104.9945
SW53_16		87.0486	0.2204	0.0000	0.2078	0.0162	0.0000	11.7418	99.2348
SW53_17		86.3258	0.3888	0.0000	0.0000	0.0000	0.0000	11.5494	98.2640
SW53_18		79.1629	0.1449	0.1481	0.7007	0.2964	0.0645	10.9526	91.4701
SW53_19		82.7457	0.3229	0.1174	0.9411	0.0533	0.0000	11.3714	95.5518
SW53_20		79.4330	0.1435	0.3936	0.9030	0.3638	0.0000	11.1332	92.3701
SW53_21		80.5302	0.4185	0.1268	9.4748	0.0000	0.0000	13.1876	103.7379
SW53_22		88.1467	0.1816	0.0000	0.1520	0.0104	0.0982	11.8904	100.4793
SW53_23		83.5497	0.2231	0.1187	0.2805	0.0023	0.0000	11.3218	95.4961
SW53_24		78.4476	0.0585	0.2240	0.8361	0.1459	0.0000	10.8860	90.5981
SW53_25		84.2848	0.2115	0.0000	0.1976	0.0000	0.0000	11.3640	96.0579
SW53_26		86.6005	0.3157	0.0166	0.1149	0.0243	0.0436	11.6475	98.7631
SW53_27		63.7545	0.0041	0.0000	38.9240	0.4774	0.0085	18.5314	121.6999
SW53_28		70.1890	0.0026	0.0747	0.0806	33.9766	0.0004	19.2396	123.5635
SW53	101	101.4609	0.0235	0.0442	1.2907	0.0511	0.0000	14.0258	116.8962
SW53	102	102.4949	0.0166	0.0000	0.0000	0.0000	0.1030	13.8210	116.4355
SW53	103	101.4454	0.0226	0.0056	0.0778	0.0000	0.1074	13.6999	115.3587
SW53	104	99.4094	0.0055	0.0032	1.0103	0.0166	0.0000	13.6597	114.1047
SW53	105	80.4632	0.0129	0.0696	0.1603	0.1270	0.0000	10.9429	91.7759
SW53	106	6.1922	0.0000	53.0737	0.2248	45.7682	0.0000	31.0050	136.2639
SW53	107	83.4873	0.0000	12.4350	0.3260	8.9782	0.0563	17.8965	123.1793
SW53	108	7.7727	0.0097	51.7526	1.0938	44.1015	0.0041	30.5343	135.2687
SW53	109	4.5402	0.0194	52.8818	0.6879	45.8664	0.0000	30.8612	134.8569
SW53	110	69.4303	0.0184	0.1572	33.8532	0.0432	0.0000	17.9418	121.4441
SW53	111	77.2059	0.0351	0.0245	24.4421	0.0515	0.0000	16.5766	118.3357
SW53	112	65.1563	0.0141	0.0000	41.3091	0.0972	0.0000	19.2090	125.7857
SW53	113	19.9707	5.3059	0.0000	0.0891	0.0876	0.0895	1.5493	27.0921
SW53	114	86.7343	0.0024	0.0017	0.8626	16.9681	0.0172	16.7720	121.3583
SW53	115	100.8079	0.0110	0.0000	0.3594	0.0000	0.0134	13.6784	114.8701
SW53	116	100.0935	0.0000	0.0000	0.1708	0.0000	0.0334	13.5386	113.8363
SW53	117	100.5480	0.0028	0.0000	0.1197	0.0000	0.1003	13.5916	114.3624
SW53	118	71.4502	20.2769	0.2170	0.0000	0.0707	0.0430	5.1494	97.2072
SW53	119	71.2751	20.8165	0.0252	0.0000	0.0000	0.0066	4.9195	97.0429
SW53	120	70.7429	20.4145	0.0780	0.0000	0.0464	0.0463	4.9718	96.2999
SW53	121	71.0669	17.6693	0.0090	0.0236	0.0000	0.0000	5.6019	94.3707
SW53	122	71.4391	19.7353	0.0000	0.2256	0.0000	0.0497	5.2377	96.6874
SW53	123	64.1594	0.0293	0.0000	42.4577	0.0732	0.1310	19.3637	126.2143
SW53	124	81.6743	0.1013	0.0288	0.2255	0.0285	0.0468	11.0650	93.1702
SW53	125	78.4035	0.0608	0.0096	0.2097	0.0190	0.0502	10.6206	89.3734
SW53	126	85.7429	0.1840	0.0000	0.0211	0.0000	0.0000	11.5223	97.4703
SW53	128	75.9177	0.0856	0.0721	0.3445	0.7915	0.4292	10.5845	88.2251

VITA

Stacie E. Dunkle, daughter of Dr. and Mrs. Chad Dunkle, was born in Cincinnati, Ohio on January 25, 1978. In May of 2000, Stacie graduated *magna cum laude* from Vanderbilt University in Nashville, Tennessee with a Bachelor of Science degree in Honors in Geology.

In August of 2000, the author was admitted in to the Department of Geological Sciences at Virginia Polytechnic Institute and State University to pursue a Master of Science degree. During her time at Virginia Tech, she was a graduate teaching assistant for four semesters, instructing labs in resource geology.

Publications

Dunkle, S.E., Craig, J.R., and Lusardi, W.R. (2001) Romarchite and the corrosion of pewter artifacts. Geological Society of America, Abstracts with Program, 33 (6): A-128.